Response to Referee #1, 28.2.2017 by Thum et al.

The manuscript by Thum et al examines the use of SIF to predict GPP in coniferous forests in southern and northern Finland. The authors implement a SIF module in the JSBACH biosphere model and evaluate seasonal and spatially variability against SIF and GPP measurements at leaf, canopy, and ecosystem scale, with focus on spring and autumn transition seasons. A key innovation is the use of active leaf level fluorescence data to understand the seasonal relationship of photochemistry and fluorescence and evaluate model performance. Although many uncertainties exist in the model simulations and in understanding dependencies on environmental vs biochemical effects, the authors show good correlation of observed and simulated variables, providing some confidence for future testing and evaluation, and paving the path for future efforts to scale between leaf and canopy/ecosystem levels. In general, I found this paper interesting and innovative, but it was hard to read at times, and the objective weren't clearly established making results and discussion hard to follow. I recommend a more careful analysis of satellite observations and some general clarifying throughout, but I expect this to be an important study with a few substantial revisions.

We thank the referee for this encouraging feedback and hope we're able to provide improved version of the manuscript based on these recommendations.

Major Comments

My main concern is biasing of GOME-2 time series by filtering of negative SIF values. These data are part of the noise needed in averaging to produce a smoothly varying signal. Because the noise is fixed (0.5 mW m-2 sr-1 nm-1 as mentioned on P9 L4) and doesn't scale with signal, this technique will remove more points in fallwinter-spring when errors are large compared to signal, leading to positive cold season biases, early spring GPP onset, and underestimated seasonal amplitude. This should explain why observed SIF doesn't reach zero level (P13 L5) and why the authors find an opposite phase an opposite phase relationship of GPP and SIF in spring at FI-Hyy in active data (photochemical yield synchronized with SIF) compared to passive data where SIF precedes GPP. I recommend reanalyzing GOME-2 results with negative values.

We thank the referee for this insight and agree. We have thus redone the analysis with the inclusion of negative values.

The authors show that model GPP is systematically early in coniferous forests compared to ground and satellite data, a finding that is consistent with previous studies of cold limited ecosystems. I was hoping the authors could take better advantage of the multiscale observations and new model capabilities to provide explanations at biochemical and environmental levels, especially since the challenge of understanding the spring transition is listed as a motivation for the study. Some speculation is provided in the discussion (e.g., frost) but not much detail and no mention in the conclusions. I think this is an important enough result and application of new methods as to warrant further discussion. I would like to see the authors discuss what is needed to improve model representation of the spring transition. What would be the effect of seasonal PSII and thermal dissipation? Growing degree days, cold temperature days, and/or frozen soils?

What important environmental controls are included/missing in the Farquhar model?

We agree with the referee that this is one focus of the manuscript, but it has not received enough focus in the earlier version. We therefore added discussion in this topic, which is shown later. There we propose using temperature related changes to the base rates of the biochemical parameters. Here the SIF observations can be used as a valuable evaluation tool for large scale estimates.

In the end, it would be desirable to have process-based description for the cold acclimation processes to properly describe the seasonal cycle of boreal forests, as this would also enhance our skill to predict changes of the carbon cycle in future climate. However, at the moment there is lack of observations to parameterize a large scale model in this respect. The parameters related to the amount of active reaction centers and sustained non-photochemical quenching are steps to this direction, but they would need parameterization in order to be useful in large scale models.

Additionally, also other processes play part. It has been suggested, that slow recovery of Rubisco has influence in spring recovery (Monson et al., 2005). It might not be possible to include all the factors in models, but combining observations and modelling efforts at different scales will hopefully reveal, which processes are most important to be included.

The spring recovery of the forests to its full summertime capacity is a gradual process (Bergh et al., 1998), that can be tracked with several environmental and biological variables (Thum et al., 2009). Air temperature is quite good proxy to be used (e.g. Thum et al., 2009), but the averaged temperature indices might benefit from inclusion of delay due to night frosts (Thum et al., 2017), that might even reverse spring recovery (Ensminger et al., 2004).

Large-scale observations can be very useful, since earlier studies (e.g. Walther et al., 2016) have shown that the temperature sensitivities differ between different regions. This study is a first step in doing that work with more extensive remote sensing data available soon. However, also more data-based approaches are valuable (e.g. Luus et al., 2017, Walther 2016) as they are increasing our understanding of the carbon cycle.

I am also interested in further elaboration of results in autumn at FI-Hyy, in particular, why F' and photochemical yield are strongly delayed relative to GPP in autumn but synchronized in spring.

In earlier version the MONI-PAM results were not discussed in detail, as they've been published also elsewhere (Porcar-Castell, 2011; Kolari et al., 2014), but of course they haven't been shown in this context and therefore there is reason to further elaborate then. In the earlier version they were discussed in the discussion, but we moved these points to the Results section and added some more detail, now mentioning photoprotection of the needles and the possible differences in the electron transport rate between observation and simulation.

Minor Comments

Abstract and Conclusions – Mostly a discussion of methods and no mention of new results. I suggest discussing at least one new and interesting result from your study. Something about spring or autumn photosynthesis, or using leaf level measurements with satellite data, or comparing model simulations to active and passive fluorescence data.

We added some results, including two points: i) the ability of observed SIF to capture seasonal cycle of photosynthesis at site scale, ii) the goodness of simulated SIF values vs. observations at regional scale.

Figure 1 - Figure legend is difficult to read and it's not clear from figure or caption what is being plotted in panel (A) – legend appears to suggest fluorescence yield as solid red but text refers to photochemical yield. GPP is not shown in panel (A) as stated in caption – please correct.

The font size in the figure legend was increased to make it easier to read. The text was corrected, so that it states that the fluorescence yield is the modelled yield (shown in solid red in the figure). The caption was corrected to say that GPP is in panel B.

Figure 3 – color scheme is confusing especially with multiple variables on 1 plot. keep observations in black and models in color like in figure 1. Use same line styles for same variables (solid for GPP, dashed for SIF).

We remade the figure like suggested.

P5L10: *an indication of the fraction of electrons in the leaf that follow the ChlF pathway

Corrected.

P6L12: *is used in

Corrected.

P7L23 & P9L2: Confusion about overpass time. Here it is stated as 10:30 am but as 9:30 am in Section 2.3.2. Please clarify or correct. Also clarify what it means for the satellite overpass time to last for 100 minutes.

We sincerely apologize for the confusion and would like to explain how this happened. We briefly introduced the properties of GOME-2 in Sect. 2.3.2, where we added "at the equator" to clarify that the actual overpass time depends on the region under investigation. The wording to express the time for one revolution might have been inappropriate. We clarified this issue by rephrasing the sentence to: "..., while one revolution takes 100 minutes." In Sect. 2.2.3 we added "local solar time" in order to prevent any misunderstanding.

P10L18: I don't see the simultaneous decrease in observed GPP with F'. GPP is already declining on Day 200 while F' appears steady until Day 280. F' decrease is also much more gradual and doesn't reach its minimum until January.

This is right. We have now corrected this part in the text.

P10L25: please elaborate what is meant here - are you suggesting that in low light conditions of spring, most of the absorbed radiation goes into photochemistry thus reducing that available to fluorescence?

Apologies for having a mistake in the subscripts, making the message of the paragraph very unclear. The important message here was connected to only fluorescence yield, that in spring it is the fluorescence yield that is holding back the increase in SIF.

In low light conditions in general, the photosynthetic yield and fluorescence yield are anti-correlated. Actually, with increasing light levels, the fraction of incoming energy used for fluorescence increases and the fraction used for photosynthesis decreases (van der Tol et al., 2009). This is because when photosystem II absorbs light and primary quinone acceptor of PSII Q_A has accepted an electron, it cannot accept another electron before it has passed on the first electron to the subsequent electron carrier. Thus, the proportion of closed reaction centres lead to a reduction in efficiency of photochemistry and increase in fluorescence (Maxwell and Johnson, 2000). We don't have any data that shows different behavior for this in spring. We are sorry for the confusion, due to the wrong subscripts.

P12L1: quantify "reasonably similar" - within 10% of observations? 5%? Regression is slightly lower on average in model

Indeed, it is a good idea to concentrate on this result more deeply, as it is one of the main results of the study. For now we added uncertainties of the slopes in the table 3 and calculated the averages and standard deviations of the different cases. These are now also mentioned in the abstract.

Note, that due to the different fitting algorithm the slopes might differ slightly from the earlier values. Also, due to the inclusion of negative observed SIF values in the analysis, the slopes are not now systematically lower in the model.

P12L8: FI-Sod has lower correlations than FI-Ken.

Yes, it depends on which correlations you're looking at in Table 2. Here we were trying to refer to correlation between modelled GPP and modelled SIF, which is at least 0.92 for other sites and 0.83 for FI-Ken. To clarify this, we added "with each other" to the text.

P12L10: provide reference for peat effect on drought

We decided to replace word “peat” as “humus” as we consider it to be more appropriate term in this context and added reference.

P13L25: what is the magnitude and direction of the seasonal drift in GOME-2 overpass, and what is the likely influence?

Although there are indeed (minor) seasonal variations in the local solar time of GOME-2 overpasses (slightly earlier during NDJ; 10:15 during winter, 10:45 during summer), we do not expect a dramatic influence, because of the senescent vegetation during this period. After including also negative values (as suggested by referee), we obtain SIF values close to zero as it can be anticipated and removed the concerned sentence accordingly. However, the morning overpass of GOME-2 leads to challenging measurement conditions (inclined solar angles) during the winter (mentioned in P14L1).

Inclined solar angles lead to longer photon path lengths, in which case rotational Raman scattering could fill in solar Fraunhofer lines. This might interfere with the SIF retrieval, which relies on the in-filling of Fraunhofer lines. We included these measurements anyways to be able to present a continuous time series (again: we observe SIF values close to zero during winter).

P14L13: please explain what a static temperature response is, the effect on early GPP, and how this could be corrected in the model

We added the following text here:

“*The photosynthesis of forests is often modelled using constant temperature response for the biochemical model parameters* V_{max} *and* J_{max} *throughout the year. However, studies have revealed that this assumption does not hold for ecosystems with strong seasonal cycles, but causes overestimation of* CO_2 *fluxes in transition periods. Kolari et al. (2014) found seasonally varying values for leaf level for those parameters from leaf level observations at FI-Hyy. Ueyama et al. (2016) found seasonally varying biochemical model values at four different black spruce forests in Alaska in a model inversion study at eddy covariance sites. In an earlier study using inversion at boreal coniferous forests (Thum et al., 2008), it was found that three forests at northern boreal zone (FI-Hyy, FI-Sod and FI-Ken) had temporal evolution in the biochemical parameters, but a site located on temperate boreal (Norunda, Sweden) did not.*

Leaf level studies have used temperature acclimation for the changes of biochemical parameters (Wang et al., 1996). Similar results have been obtained for site level results at FI-Sod, where dark acclimated chlorophyll fluorescence observations have been used in combination with eddy covariance observations to disentangle the effect of changing maximum photosynthetic capacity (Thum et al., 2017).

The changes taking place in the needles of conifer forests in winter are numerous to protect the needles in challenging environmental conditions. E.g. the light harvesting complexes are aggregated (Porcar-Castell, 2011) and the xanthophyll cycle enables photoprotection (Ensminger et al., 2004). Some of these processes can be in future be included in a large scale model, as adding changes to the parameters in the ChlF model discussed below, but as changes in the boreal spring happen at quite fast pace and those can be tracked with several different environmental and biological variables (Thum et al., 2009), for large scale applications a temperature related changing of the biochemical parameters might be next step forward and remotely sensed SIF observations provide a very useful evaluation tool in this context."

P15L4: add condition "assuming a homogeneous landscape"

We guess that this was meant for page 16… We made the addition there.

References

Bergh, J., McMurtrie, R. E., and Linder, S.: Climatic factors controlling the productivity of Norway spruce: a model-based analysis, Forest Ecol. Manag., 110, 127–139, 1998.

Ensminger, I., Sveshnikov, D., Campbell, D. A., Funk, C., Jansson, S., Lloyd, J., Shibistova, O., and Öquist, G.: Intermittent low temperatures constrain spring recovery of photosynthesis in boreal Scots pine forests, Global Change Biol., 10, 995–1008, 2004.

Luus, K. A., et al. (2017), Tundra photosynthesis captured by satellite-observed solar-induced chlorophyll fluorescence, Geophys. Res. Lett., 44, doi:10.1002/2016GL070842.

Monson R.K., Sparks, J.P., Rosenstiel, T.N., Scott-Denton, L.E., Huxman, T.E., Harley, P.C., Turnipseed, A.A., Burns, S.P., Backlund, B., and Hu J.: Climatic influences on net ecosystem CO_2 exchange during the transition from wintertime carbon source to springtime carbon sink in a high-elevation, subalpine forest, Oecologia, 146, 130–147, 2005.

Norton, A. J., Rayner, P. J., Koffi, E. N., and Scholze, M.: Assimilating solar-induced chlorophyll fluorescence into the terrestrial biosphere model BETHY-SCOPE: Model description and information content, Geosci. Model Dev. Discuss., doi:10.5194/gmd-2017-34, in review, 2017.

Thum, T., Aalto, T., Laurila, T., Aurela, M., Hatakka, J., Lindroth, A., and Vesala, T.: Spring initiation and autumn cessation of boreal coniferous forest CO_2 exchange assessed by meteorological and biological variables, Tellus 61B, 701-717, 2009.

Thum, T., Aalto, T., Aurela, M., Laurila, T., and Zaehle, S.: Improving the modeling of the seasonal carbon cycle of the boreal forest with chlorophyll fluorescence measurements, in preparation, 2017.

Ueyama, M., Tahara, N., Iwata, H., Euskirchen, E.S., Ikawa, H., Koyayashi, , Nagano, H., Nakai, T., and Harazono, Y.: Optimization of a biochemical model with eddy covariance measurements in black spruce forests of Alaska for estimating CO_2 fertilization effects, Agr. Forest Meteorol., 222, 98-111, 2016.

Wang, K. Y., Kellomäki, S., and Laitinen, K.: Acclimation of photosynthetic parameters in Scots pine after three-year exposure to elevated CO_2 and temperature, Agr. Forest Meteorol., 82, 195–217, 1996.

Response to Referee #2, 28.2.2017 by Thum et al.

The authors use GPP data derived from CO2 fluxes measured at 4 boreal forest sites, together with SIF derived from the GOME satellite and leaf-level active fluorescence data to test a new version of the land surface model JS-Bach, which has been updated with a description of ChlF fluorescence. Finally, JS-Bach is applied at regional scale.

The authors demonstrate overall good correspondence between measured and simulated GPP (which was calibrated though) and satellite SIF and site-level GPP and reasonable correspondence to leaf-level active fluorescence data. SIF compares better to measured GPP compared to remotely sensed fAPAR.

I think this is a useful and original contribution. My comments are mostly meant to improve clarity, which the ms frequently lacks.

We thank the referee for these comments and hope that our responses to the comments are able to clarify the manuscript.

Detailed comments:

p. 3, l. 6: as ecosystems exchange various forms of carbon, use carbon dioxide if you actually refer to carbon dioxide

Indeed, the aim was here to refer only to carbon dioxide, not to methane or VOCs, so we made this addition to clarify the text.

p. 3, l. 11: strictly speaking this is only true for fAPAR, while NDVI is just the normalized difference between reflectances in NIR and red, which happens to correlate with fAPAR

We totally agree with the referee and this was a language issue. We replaced “which” by “describing”, hopefully now clarifying the issue.

p. 4, l. 1: I would contradict the “readily”, given that we are still far from a truly process-based description of SIF; the Farquhar model though offers most of the interfaces for coupling to SIF

We agree with the referee. We took away the word “readily”.

p. 4, l. 12: “Both these regions . . .”

Thank you, this is now corrected in the text.

p. 4, l. 15-15: here you might explain why you focus on spring and autumn

A good point. We added here the following text: “*Forests in the boreal zone experience strong seasonal cycle with cold winters and warm summers (Bonan, 2008). The transition periods of spring and autumn influence the carbon balances in these northern ecosystems (Bergh et al., 1998). In changing climate the conditions in spring and autumn will change (Ruosteenoja et al., 2011)and cause changes to carbon balances. It is anyhow during these times that the carbon cycle models have difficulties in performance (Schaefer et al., 2012). Therefore it is important to find ways to improve carbon cycle models in these time periods.”*

p. 4, l. 19: here you haven’t mentioned yet that you did implement SIF into your LSM

Thank you, we changed the text so that we separately mention the implementation.

p. 4-5, section 2.1: while this section clarifies some of the basics, it entirely lacks details, such as which instrument was used for active measurements in the field and how the experimental protocol was, etc. – I see this comes later, so an appropriate header reflecting this is required here

A good point again, we added “in general” to the title in order to clarify the issue.

p. 6, l. 6-7: the acronyms/abbreviations do not make sense – maybe use subscripts like dir and dif to distinguish between direct (beam) and diffuse radiation;

Indeed, the used abbreviations were not that clear. We used referee’s suggestion to distinguish between direct and diffuse radiation.

Wouldn’t the equation be easier to understand if fAPAR was calculated as the difference between the radiation balance at the top of canopy (layer 1) minus the radiation balance below the lowermost layer (layer 3);

We understand the referee’s point, but we have a three –layer canopy and here we wanted to show how to calculate fAPAR for each layer. As said in the text, the canopy fAPAR is the sum of fAPAR from different layers.

replace “transmitted” by “used” or similar

We made that.

p. 6, l. 12: “. . . is used ..”

Thank you, corrected.

p. 6, l. 16: typically the temperature dependency of Jmax is either exponential or even follows an optimum shape

We agree, but in this study we decided not to make any changes to the original formulation of the JSBACH model, that would have required then some additional evaluations of the model performance.

p. 6, l. 17: isn't the value of alpha typically around 0.05 (mol CO_2/mol photons)

We're talking here about apparent quantum yield, not the intrinsic quantum yield. We modified the text to say apparent quantum yield, which is the true quantum yield multiplied by the light absorption in the leaf (Walker et al., 2014). This value (0.28) is the default value of JSBACH for all the different plant functional types. The parameter optimization study by Mäkelä et al. (2016) done by JSBACH at site level for FI-Hyy and FI-Sod, showed this value to be good for the two sites.

p. 7, l. 19: "obtained" – use past tense throughout

Thank you, we corrected that.

p. 8, l. 19, 24: two times same header numbering

Thank you, we corrected that.

p. 9, l. 5: is it a good idea to introduce a bias into the data? Isn't there some other way to deal with the negative values?

We have redone the analysis by including the negative values in the analysis.

p. 9, l. 9: does this explain how fAPAR is derived? I mean in the sense that a reader should be able to repeat the author's approach?

What the author did related to fAPAR was to ask Thomas Kaminski for these data, that he kindly provided and even took out data for each site. These values were obtained by partitioning the solar radiation fluxes that were based on inversion of the MODIS broadband white sky surface albedos and the reference for those data is given here. As we did not do the laborious processing it takes to obtain those data, we did not go into details here.

p. 9, l. 18: what does "adjusted" exactly mean? Which metric did you use to measured the success of the "adjustment"?

We didn't perform here any rigorous tuning with profound mathematical methods, like done by Mäkelä et al. (2016). Instead, we matched the averaged LAI value to the observations. We did not consider building a model tuning framework for this work, as we're not dealing with the absolute GPP values from the sites, but instead we use our modelled time series to assess the seasonal behavior of the model. We added sentence: "*No rigorous parameter inversion methods were used, as we did not use the absolute GPP values in our study, but focused more on the seasonal behavior.*" to the text.

typically, Jmax is linked to Vcmax through the ratio of the two – was that done here too, i.e. only Vcmax adjusted and Jmax "followed" based on the relatively conservative ratio of the two?

Yes, the original ratio between Vcmax and Jmax was 2.1, and we kept this same ratio, by changing first Vcmax and then always Jmax accordingly. We added this point to the text.

p. 10, l. 14: what exactly means "most" in this context?

Apologies, that was unclear. We did the analysis for points having larger fraction than 0.5 for the vegetation, but plotted all the points to the map in Fig. 4. We clarified this.

p. 11, l. 1: doesn't the term "midday depression" refer to the drought-related midday decrease in leaf net photosynthesis and stomatal conductance?

Yes, we took that away, as it's not in the right context here.

p. 16, l. 2: "wider footprint" – be more precise . . .

We added (e.g. for GOME-2 default footprint is 80 km x 40 km) in parenthesis to be more explicit.

Fig. 1: might be worth commenting on the negative measured GPP values

This is a good addition. The negative values are originating from measurement uncertainty. The GPP is obtained from the observed NEE by subtracting the respiration fitted by temperature regression. The temperature fit to respiration adds some systematic error to the GPP estimate. We wrote to the manuscript:

"*Some negative GPP values are present in Fig. 1. The random nature of turbulence and instrument uncertainty add to measurement uncertainty (Rannik et al., 2016). The GPP is obtained from the observed net ecosystem exchange (NEE) by subtracting the respiration that has been estimated by a regression fit to temperature (Wohlfahrt and Galvano, 2017). Thus the random measurement uncertainty leads to some negative GPP values that are compensated by equal amount of too high positive values, additionally the temperature fit to respiration causes some systematic error in the values.*"

References

Bergh, J., McMurtrie, R. E., and Linder, S.: Climatic factors controlling the productivity of Norway spruce: a model-based analysis, Forest Ecol. Manag., 110, 127–139, 1998.

Bonan, G.B.: Forests and climate change: Forcings, feedbacks, and the climate benefits of forests, Science, 320, 1444–1449, 2008.

Mäkelä, J., Susiluoto, J., Markkanen, T., Aurela, M., Järvinen, H., Mammarella, I., Hagemann, S., and Aalto, T.: Constraining ecosystem model with adaptive Metropolis algorithm using boreal forest site eddy covariance measurements, Nonlin. Processes Geophys., 23, 447-465, doi:10.5194/npg-23-447-2016, 2016.

Rannik, Ü., Peltola, O., and Mammarella, I.: Random uncertainties of flux measurements by the eddy covariance technique, Atmos. Meas. Tech., 9, 5163-5181, doi:10.5194/amt-9-5163-2016, 2016.

Ruosteenoja, K., Raisanen, J. and Pirinen, P.: Projected changes in thermal seasons and the growing season in Finland, Int. J. Climatol., 31, 1473–1487, 2011.

Schaefer, K., et al.: A model-data comparison of gross primary productivity: Results from the North American Carbon Program site synthesis, J. Geophys. Res., 117, G03010, doi:10.1029/2012JG001960, 2012.

Walker A. P., Beckerman A. P., Gu L., Kattge J., Cernusak L. A., Domingues T. F., Scales J. C., Wohlfahrt G., Wullschleger S. D., Woodward F. I. (2014) The relationship of leaf photosynthetic traits – Vcmax and Jmax - to leaf nitrogen, leaf phosphorus, and specific leaf area: a meta-analysis and modeling study. Ecology and Evolution 4, 3218-3235, doi: 10.1002/ece3.1173.

Wohlfahrt, G. and Galvano, M.: Revisiting the choice of the driving temperature for eddy covariance CO_2 flux partitioning, Agric. Forest. Met., 237-238, 135-142, 2017.

A list of all relevant changes in the manuscript

- All figures (except Fig. 2) have been updated (Fig. 1 due to the comments and Figures 3-7 due to the inclusion of negative values in the analysis).
- Tables 2 and 3 were updated with regard to the change in the analysis, also corresponding parts in the Results-section were modified. To Table 3 we also added uncertainties of the slopes, average slopes and their standard deviations.
- Discussion on early peaked behavior of the SIF signal has been removed from the text and from the supplement 2, as this was no longer issue when the negative values were included in the analysis.
- In the Introduction we added some motivation of why seasonality is important in studying boreal forests.
- We added more text to Section 3.1, so that the seasonal cycle of chlorophyll fluorescence variables is more thoroughly discussed and also the negative GPP values are now mentioned.
- We added text to the discussion about the seasonality and how it could be modelled.

Modelling sun-induced fluorescence and photosynthesis with a land surface model at local and regional scales in northern Europe

Tea Thum[1], Sönke Zaehle[2], Philipp Köhler[3], Tuula Aalto[1], Mika Aurela[4], Luis Guanter[3], Pasi Kolari[5], Tuomas Laurila[4], Annalea Lohila[4], Federico Magnani[6], Christiaan Van Der Tol[7],Tiina Markkanen[1]

[1]Climate Research, Finnish Meteorological Institute, P.O. Box 503, 00101 Helsinki, Finland
[2]Biochemical Integration Department, Max Planck Institute for Biogeochemistry, Hans-Knöll-Str. 10, 07745 Jena, Germany
[3]Helmholtz-Centre Potsdam, GFZ German Research Centre for Geosciences, Section 1.4 Remote Sensing, Telegrafenberg, 14473 Potsdam, Germany
[4]Atmospheric Composition Research, Finnish Meteorological Institute, P.O. Box 503, 00101 Helsinki, Finland
[5]Department of Physics, University of Helsinki, 00014 University of Helsinki, Finland
[6]University of Bologna, Via Zamboni, 33, 40126 Bologna, Italy
[7]Deparment of Water Resources, Faculty ITC, University of Twente, P.O. Box 217, 7500 AE Enschede, Netherlands

Correspondence to: Tea Thum (tea.thum@fmi.fi)

Abstract. Recent satellite observations of sun-induced chlorophyll fluorescence (SIF) are thought to provide a large-scale proxy for gross primary production (GPP), thus providing a new way to assess the performance of land surface models (LSMs). In this study, we assessed how well SIF is able to predict GPP in the Fenno-Scandinavian region and what potential limitations for its application exist. We implemented a SIF model into the JSBACH LSM and used active leaf level chlorophyll fluorescence measurements (ChlF) to evaluate the performance of the SIF module at a coniferous forest at Hyytiälä, Finland. We also compared simulated GPP and SIF at four Finnish micrometeorological flux measurement sites to observed GPP as well as to satellite observed SIF. Finally, we conducted a regional model simulation for the Fenno-Scandinavian region with JSBACH and compared the results to SIF retrievals from the GOME-2 (Global Ozone Monitoring Experiment-2) space-borne spectrometer and to observation-based regional GPP estimates. Both observations and simulations revealed that SIF can be used to estimate GPP at both site and regional scales. At regional scale the model was able to simulate observed SIF averaged over five years with r^2 of 0.86. The GOME-2 based SIF was a better proxy for GPP than the remotely sensed fAPAR (fraction of absorbed photosynthetic active radiation by vegetation), even though high SIF values occurred during early spring at the northern latitudes, although these are not likely to be associated with photosynthesis. .The observed SIF captured the seasonality of the photosynthesis at site scale and showed feasibility for use in improving of model seasonality at site and regional scale.

List of abbreviations

Φ_f - Quantum yield of fluorescence [quanta emitted / quanta absorbed]

$\Phi_{f,s}$ – Scaled quantum yield of fluorescence [quanta emitted / quanta absorbed]

Φ_p – Quantum yield of photochemistry in PSII [electrons transported / quanta absorbed]

ChlF – chlorophyll fluorescence (general term)

ESM – Earth System Model

EVI – Enhanced Vegetation Index

F' – Prevailing fluorescence signal as measured with PAM fluorometry [relative units, e.g. sensor mV output]

fAPAR – Fraction of absorbed photosynthetic active radiation by vegetation

FTS - Fourier Transform Spectrometer; spectrometer on GOSAT satellite

GOME-2 – Global Ozone Monitoring Experiment-2; spectrometer on MetOp-A (Meteorological Operational Satellites) satellite

GOSAT – Greenhouse Gases Observing Satellite

GPP – Gross Primary Production

JSBACH – Jena Scheme for Biosphere Atmosphere Coupling in Hamburg; the land surface model of the Max Planck Institute's Earth System Model

LSM – Land Surface Model

NDVI - Normalized Difference Vegetation Index

PAR – Photosynthetically active radiation

PSII – Photosystem II

SCIAMACHY - SCanning Imaging Absorption SpectroMeter for Atmospheric CHartographY; spectrometer on ENVISAT (ENVIronmental SATellite) satellite

SCOPE - Soil-Canopy Observation of Photosynthesis and Energy

SIF – Sun-induced fluorescence [e.g. in W m^{-2} sr^{-1} nm^{-1}], obtained from passive observations or from a model

1 Intoduction

The terrestrial biosphere is thought to store approximately a quarter of the carbon dioxide (CO_2) released by anthropogenic activity (Le Quéré et al., 2016). However, a detailed spatio-temporal distribution of this uptake is absent, partly due to an incomplete understanding of the terrestrial carbon balance as a whole. Estimates of the terrestrial net carbon balance are often made by land surface models (LSMs) (Sitch et al., 2015). However, assessing and improving the performance of LSMs at larger scales remains a challenge, as limited data sources for large scale carbon dioxide flux estimates are available (Luo et al., 2012). Increasing our knowledge of carbon dioxide uptake will thus help to provide better estimates of the global carbon balance.

Previous global estimates of the spatial distribution and the variability of plant photosynthetic production have mostly been based on remote sensing of vegetation greenness (such as the normalized difference vegetation index, NDVI) or the fraction of absorbed radiation (fAPAR)~~,~~ ~~which~~ describing~~es~~ how much of the incoming photosynthetically active radiation (PAR) is absorbed by the vegetation (Pinty et al., 2011). Recently, global retrievals of sun-induced fluorescence (SIF) have also become available for the monitoring of global vegetation productivity (e.g. Frankenberg et al., 2011, Joiner et al., 2011).

Chlorophyll fluorescence (ChlF) takes place in plant leaves when they photosynthesize. The light energy absorbed by the chlorophyll molecules is used in photosynthesis, dissipated as heat or re-emitted as light through ChlF (Maxwell and Johnson, 2000). Thus, ChlF correlates with two simultaneous processes: photosynthesis and heat dissipation. Therefore, ChlF has been a standard measurement at the leaf scale in plant physiology for decades (Baker, 2008). The advent of retrieval approaches for satellite data acquired by the spectrometers FTS (onboard satellite GOSAT), SCIAMACHY (satellite ENVISAT), GOME-2 (satellite MetOp-A and B) and OCO-2 have demonstrated that it is possible to measure SIF from space (e.g. Frankenberg et al., 2011, 2014; Guanter et al., 2012, Joiner et al., 2012, 2013; Köhler et al. 2015).

As the seasonal cycles of fAPAR and SIF are related to radiation and greenness of the vegetation, they appear similar in many ecosystems. However, SIF is more physiologically related to photosynthesis and has been shown to track gross primary production (GPP) better than fAPAR in deciduous broadleaf and mixed forests as well as in croplands (Joiner et al., 2014). Moreover, comparison to observation-based upscaled global GPP products (Jung et al., 2011) has suggested that SIF is a better estimator of GPP than other traditional remotely sensed vegetation indices, such as EVI (enhanced vegetation index) and NDVI (Frankenberg et al., 2011; Walther et al., 2016), and may thus be of relevance in the observation or modelling of the terrestrial carbon balance (Lee et al., 2015; Parazoo et al., 2013).

SIF can be ~~readily~~ estimated from state-of-the-art photosynthesis models, such as the widely used Farquhar model (Farquhar et al., 1980), by describing the processes of photosynthesis and fluorescence at the cellular level (van der Tol et al., 2009a), or leaf level (van der Tol et al., 2014). The strong dependence of the measurable SIF signal on scattering and reabsorption effects within the canopy requires explicit formulation of the radiative transfer (e.g. SCOPE; van der Tol et al. 2009b). Nevertheless, modelling studies using satellite observed SIF have revealed links between forest productivity and water stress in the Amazon (Lee et al., 2013) and have helped to constrain the seasonal cycle of GPP (Parazoo et al., 2014). Koffi et al. (2015) included SIF in their global carbon cycle data assimilation system and found SIF to be more sensitive to the chlorophyll content in the leaves than to the parameter maximum carboxylation rate controlling model GPP.

The challenge in using the space-borne SIF data for the evaluation of SIF models is the lack of similar ground-based observations, and the degree of correspondence between GPP and SIF at different spatial scales. Another important consideration is that the SIF observation from space is dependent on a passive measurement carried out in narrow spectral bands. The signal in the red region originates mostly from the top of the canopy, whereas deeper canopy layers also contribute to the far-red signal (Porcar-Castell et al., 2014). ~~These b~~Both these regions can be used in retrieving SIF from remote sensing observations.

Our aim in this study is to assess whether the SIF measurements can be used to quantify the LSM performance at a regional scale for the spring and autumn transition periods. Forests in the boreal zone experience strong seasonal cycle with cold winters and warm summers (Bonan, 2008). The transition periods of spring and autumn influence the carbon balances in these northern ecosystems (Bergh et al., 1998). In changing climate the conditions in spring and autumn will change (Ruosteenoja et al., 2011) and cause changes to carbon balances. It is anyhow during these times that the carbon cycle models have difficulties in performance (Schaefer et al., 2012). Therefore it is important to find ways to improve carbon cycle models in these time periods.

~~The focus of this study is on Fenno-Scandinavia, a region characterized by pronounced seasonal changes in photosynthesis~~. In Fenno-Scandinavia~~this study region,~~ coniferous forests are very common and study of their photosynthetically active period with remote sensing products is a challenge because of the stronger relative contribution to the GPP cycle of the physiological seasonal cycle than the changes in green foliage area (Böttcher et al., 2014). Our strategy consists of implementing ~~testing the implemented~~ a ChlF model into LSM JSBACH model and evaluating the results of this implementation~~of our LSM JSBACH model~~. We examined the performance of the model by comparing it to leaf-level ChlF observations at the site scale in one forest. We then evaluated the model performance at four coniferous forest sites by comparing the remotely sensed SIF signal from GOME-2, modelled SIF and the modelled GPP to observations with the eddy covariance technique. Finally, we made a regional model run for Fenno-Scandinavia and compared our results to satellite observations.

2 Materials and methods

2.1 Active and passive measurements of ChlF in general

Active measurements of ChlF in field conditions are typically done with the pulse amplitude modulated (PAM) technique where ChlF is measured over a broad spectral region (Porcar-Castell et al., 2014). In the active measurement, a weak and pulsed measuring light is used to excite fluorescence. The ChlF measured by PAM is not dependent on the prevailing light environment, but reflects the efficiency in transforming the measuring light into fluorescence. The active measurement provides the fluorescence signal F' and the photosynthesis yield Φ_p, which describes the fraction of absorbed photons used in photosynthesis. For the separation between non-photochemical quenching (NPQ) (i.e.heat dissipation) and Φ_p it is also necessary to have observations of dark-adapted leaf, as it is assumed that dark-adapted leaf with all the reaction centers open do not exhibit NPQ (Murchie and Lawson, 2013).

Passive measurements are an alternative to active observation of ChlF and rely on the emission under natural light environments, where the SIF is estimated in very narrow spectral bands and is affected by ambient illumination (Porcar-Castell et al., 2014). Passive measurements can be ground-based, but also based on remote sensing carried out on the ground or from space (Meroni et al., 2009). Passive observations rely on the in-filling of atmospheric or solar absorption lines by SIF. The ChlF yield (Φ_f) can be obtained from the passive measurements and it is an indication of the how big fraction of electrons in the leaf follow the ChlF pathway.

Thus, passive measurements provide SIF and fluorescence yield Φ_f values, whereas the active measurements provide the prevailing fluorescence signal F' and yield of photosynthesis Φ_p. In non-stressed low light conditions most of the absorbed energy is used for photosynthesis (causing higher Φ_p) that results in lower fluorescence yield (Φ_f). Therefore an inverted relationship exists between ChlF and photosynthesis yields at low light levels (van der Tol et al., 2009a). However, during high light and/or stressed conditions NPQ is increased and then Φ_p and Φ_f are positively correlated.

2.2 Models

2.2.1 JSBACH

We used the biosphere model JSBACH (Reick et al., 2013) that is part of the Max Planck Institute's Earth System Model (Giorgetta et al., 2013). In addition to the global simulations, JSBACH can also be applied at regional and site scales.

The JSBACH model simulates the exchanges of carbon, water and energy between the land surface and the atmosphere. The incoming radiation that reaches the canopy is calculated for the three different canopy layers a using two-stream approximation model (Dickinson 1983, Sellers 1985). In this model, it is assumed that the distribution of scattering objects in the canopy is homogenous so that the radiation distribution inside the canopy is horizontally invariant. Therefore, it is necessary to only consider vertical radiant fluxes.

Fraction of absorbed PAR (fAPAR) for one layer is calculated as

$$fAPAR(l_n, l_{n+1}) = \frac{I_{tot}(l_n) - I_{tot}(l_{n+1})}{R_{dirt}(0) + R_{diff\downarrow t}(0)} \quad (1)$$

where l_n is the cumulative leaf area index (LAI) for the canopy layer, I_{tot} is the total incoming radiation that reaches the canopy layer and includes the direct incoming radiation to the canopy layer and upward and downward diffuse radiation. $R_{tdir}(0)$ is the direct radiation at the top of the canopy and $R_{\downarrow t diff}(0)$ is the incoming diffuse radiation at the top of the canopy. The absorbed radiation for each canopy layer is further used intransmitted to the photosynthesis calculation. The fAPAR for the whole canopy is obtained by summing the values from the three different layers together.

In this model, photosynthesis is described by the Farquhar *et al.* (1980) formulation for C3 plants and stomatal conductance is based on Knorr (2000) (photosynthesis for C4 plants follows Collatz et al. (1992) but these species are not relevant in our study region). Photosynthesis is either electron transport rate or maximum carboxylation rate limited. The electron transport rate J from the photosynthesis model is used in the calculation of chlorophyll fluorescence and its formulation is as follows:

$$J(I) = J_{max} \frac{\alpha I}{\sqrt{J_{max}^2 + \alpha^2 I^2}} \quad (2)$$

where J_{max} is the maximum electron transport rate (unit: µmol m^{-2} s^{-1}) with a linear air temperature dependency, I is incoming photosynthetically active radiation (unit: µmol m^{-2} s^{-1}) and α is the apparent quantum yield efficiency of photon capture (value 0.28).

The vegetation in JSBACH is described by Plant Functional Types (PFTs). Different PFTs have specific physiological properties, such as photosynthetic capacity and physical properties, such as the albedo of the canopy. Each grid cell can contain up to four different PFTs and we used 13 potentially different PFTs for vegetation in our simulation. The vegetation map was based on the European Corine Database, described in Törmä et al. (2015). The leaf area development in JSBACH is based on the LoGro-P (Logistic Growth Phenology) model (Böttcher et al., 2016). Air temperature is the main driver of the phenological development in the two main vegetation types (evergreen needleleaf forests and temperate deciduous broadleaf forests) in our study region.

2.2.2 Leaf-level chlorophyll fluorescence

The model equations for the leaf-level fluorescence are shown in Appendix A. The outputs of the model are SIF and scaled fluorescence yield $\Phi_{f,s}$. Due to simplifying assumptions such as lack of wavelength separation we do not simulate the magnitude of SIF with JSBACH. However, seasonal changes in the modelled SIF are still captured. In the ChlF related literature, the ChlF quantities are often referred to as parameters, but in this work the word parameter will refer to a model parameter that is kept constant and ChlF related observations are instead referred to as variables.

2.2.3 Canopy scaling

In order to derive a comparatively simple, computationally efficient scheme for the emission and extinction of radiation in the fluorescence wavelengths, we developed a simplified parameterization with the form

$$SIF_{can} = \sum_{i=1}^{n_{layers}} SIF_i \cdot e^{\left(-k_{fl} \frac{LAI_{tot}}{n_{layers}} \cdot i\right)} \qquad (3)$$

where SIF_{can} refers to the SIF signal that originates from the whole canopy, n_{layers} is the number of canopy layers in JSBACH, k_{fl} is the attenuation coefficient, LAI_{tot} is the total LAI of the canopy. This equation is based on the output of the comprehensive radiative transfer model SCOPE and describes the radiative transfer, photosynthesis, chlorophyll fluorescence, temperature and energy balance at site-level for a given canopy structure (van der Tol et al., 2009b).

We used the SCOPE model version 1.52b in our study. We derived the parameterization of equation (3) by first calculating the hemispherically integrated top of the canopy value for SIF when emission was coming from only one canopy layer at a time. Thus we obtained a profile of how much of the emission that originated~~s~~ from each canopy layer reached~~s~~ the top of the canopy. Dividing this profile by the emission of the different layers yielded~~s~~ the attenuation of the ChlF signal in the canopy. The derived attenuation coefficient k_{fl} was slightly sensitive to the wavelength considered, while changing the amount of foliar mass/area did not affect the attenuation coefficient. The attenuation coefficient k_{fl} also varied with the solar hourly angle: k_{fl} for wavelength 740 nm was 0.350 at noon and 0.347 at 10:30 am, which corresponds to the approximate local solar time of the GOME-2 observation. Therefore, we used the attenuation coefficient k_{fl} value 0.347 in our analysis.

2.3 Measurements

2.3.1 Site level ChlF and carbon dioxide (CO_2) flux measurements at Hyytiälä

The ChlF site level measurements are from a Scots pine (*Pinus sylvestris*) forest at Hyytiälä, Finland (61°51ˈN, 24°17ˈE, 180 m a.s.l.) (Kolari et al., 2009). The forest was planted in 1962 after burning and mechanical soil preparation. The soil is a Haplic Podzol on glacial till and the site is of medium fertility (Kolari et al., 2009). The forest also has a sparse understory of Norway spruce (*Picea abies*). The total leaf area index (LAI) is 6 m^2 m^{-2} for the Scots pine. The CO_2 flux between the vegetation and the atmosphere was measured continuously with a closed-path eddy covariance system that is described in more detail in Rannik et al. (2004) and Mammarella et al. (2009). Gapfilling and flux partitioning are described in Kolari et al. (2009).

ChlF was measured in the Scots pine needles with a MONITORING-PAM Multi-Channel Chlorophyll Fluorometer (Walz, Effeltrich, Germany) (Porcar-Castell et al., 2008; Porcar-Castell, 2011). The measurement period was 15.8.2008 – 14.8.2009. The measurement system MONI-PAM uses a modulated blue LED light to measure the fluorescence emitted from the leaf sample (Porcar-Castell, 2011). We used the results from an emitter-detector unit that measured three or four pairs of needles arranged in a leaf clip. The unit was located in the mid-canopy.

The instrument recorded instantaneous fluorescence (F'), maximal fluorescence (Fm') and incident PAR radiation. During nighttime, the maximal fluorescence (Fm) and the minimal fluorescence (F_o) were measured. The observations were done every 10 minutes during summer and every 30 minutes during winter. The temperature sensitivity of the LED measuring light was corrected in the absolute fluorescence levels (Porcar-Castell, 2011). From the measured ChlF variables it was possible to calculate the quantum yield of PSII by $\Phi_p = (Fm' - F') / Fm'$.

2.3.2 Other CO_2 flux measurement sites

In addition to Hyytiälä (FI-Hyy), we used measurements from three other Finnish flux measurement sites. Together these four sites cover a wide latitudinal range, with the two southern sites; Hyytiälä and Kalevansuo(FI-Kns) located in the southern boreal zone. Two sites are located north of the Arctic Circle; Sodankylä (FI-Sod) and Kenttärova (FI-Ken) in the northern boreal zone. FI-Ken is a Norway spruce forest, whereas the other sites are Scots pine forests. More site information can be found in Table 1.

2.3.3~~2~~ Observations from space, SIF and fAPAR

To obtain estimates for SIF, we used data from GOME-2 (Global Ozone Monitoring Instrument 2), which is an operational medium resolution nadir-viewing UV/visible and near-infrared cross-track scanning spectrometer on-board EUMETSAT's polar orbiting MetOp-A and B (Meteorological Operational Satellites) (Munro et al., 2006). The spectrometer measures the Earth's backscattered radiance and the extraterrestrial solar irradiance. The overpass time of the satellite is around 9:30 am local solar time at the equator, while one revolution takes~~and it lasts approximately~~ 100 minutes. Here, we use the GOME-2 SIF data set derived with the approach presented by Köhler et al. (2015). The retrieved SIF data were available for 2007-2011, with an 8-day time resolution and a spatial resolution of 0.5° x 0.5°. Typical SIF error estimates range up to 0.5 mW m^{-2} sr^{-1} nm^{-1} (Köhler et al., 2015). Negative values of observed SIF were removed from the analysis. This will likely introduce a positive bias in the values, but it did not affect the seasonal variations in the observations and thus the quantitative analysis presented here.

In our analysis, we also used the space-observed variable fraction of absorbed photosynthetically active radiation (fAPAR). These values were obtained by partitioning the solar radiation fluxes that were based on inversion of the MODIS broadband white sky surface albedos (Pinty et al., 2011). Temporal resolution was 16-days and spatial resolution one kilometer. Monthly values of fAPAR were used in the analysis.

2.4 Simulations

2.4.1 Site level simulations

At the site-level, JSBACH was run with observed half-hourly meteorology data (air temperature, shortwave and longwave radiation, specific humidity, wind speed, precipitation) for each site, and the vegetation at the site was prescribed to be an evergreen coniferous forest. ERA-Interim data (Dee et al., 2011) was used to fill the missing values in the meteorological time series. The seasonal maximum of LAI of the model over several years was matched to the observed value. The maximum carboxylation rate $V_{c(max)}$ and maximum potential electron transport rate J_{max} parameters were adjusted so that the modelled GPP matched the magnitude of the observation-based GPP. The two parameters have a fixed ratio and J_{max} was fixed accordingly. No rigorous parameter inversion methods were used, as we did not use the absolute GPP values in our study, but focused more on the seasonal behavior. In JSBACH, these two Farquhar model parameters have a vertical profile, which were here assumed to correspond to the observed vertical distribution of foliar nitrogen content (in units leaf mass per area) at FI-Hyy (Palmroth and Hari, 2001).

A comparison of leaf-scale observations with PAM to site-scale simulated values is somewhat difficult, as the PAM measurement provides the photosynthesis yield Φ_p and fluorescence signal F', whereas JSBACH includes the "passive" fluorescence yield Φ_f and when multiplied by the radiation provides an estimate of SIF. Notwithstanding these differences, the seasonal cycle of both values may be compared in relative terms as both are connected to the activity of the photosynthetic apparatus in the plants. The observed GPP is obtained from the flux tower and is, therefore, at the same scale as the simulation output.

At four micrometeorological measurement sites, the modelled SIF and GPP were compared to observed GPP and satellite observations of SIF. Averages of the 2° x 2° spatial resolution pixels closest to the flux tower from the satellite observations were used with a 20-day time period. Averages were used rather than the closest pixel to the site, as spatial averaging reduces the retrieval data error. At the northern sites some satellite observations from mid-winter were absent due to cloud contamination. Therefore those time periods were omitted from the analysis. In addition, the time period 9–11 am was taken from the model results and flux measurements to allow for comparability with the satellite observations.

2.4.2 Regional scale simulations

The modelling domain consisted of Fenno-Scandinavia (52° – 74°N, 4° – 44°E). The meteorological data for JSBACH was prepared with the regional climate model REMO (Jacob and Podzun 1997, Jacob 2001, Jacob et al., 2001), which was run with an hourly time-step driven by the six hourly boundary conditions obtained from the ERA-Interim re-analysis (Dee et al., 2011). The resolution of REMO in our set-up is 0.1667 degrees. The JSBACH regional run had the same spatial and temporal resolutions. In this study, we focused on the region 52° – 72°N, 4° – 32°E.

We made comparisons between modelled and observed SIF and also between modelled SIF and GPP and the MPI-BGC GPP product that is available at monthly time scales (Jung et al., 2009, 2011). The GPP product is data-based and has been upscaled for regional and global scales using the model tree ensemble approach. For ~~most of~~ the analysis the model grid points with less than 50% of vegetation cover were omitted.

3 Results

3.1 Annual time series of ChlF and GPP at leaf and site scale

Observed ChlF and GPP had a pronounced annual cycle at Hyytiälä forest (Fig. 1). The observed quantum yield of photosynthesis Φ_p decreased to a low winter level later than the observed fluorescence signal F'. The F' started to decrease around doy 280, later than the observed GPP flux, which was reduced to zero around mid-November ~~The F' started to diminish simultaneously with the observed GPP flux, which was reduced to zero around mid-November.~~ The increase in observed ChlF variables; F' and Φ_p, took place at the same time in spring and this was also connected to the beginning of photosynthesis.

Simulated SIF decreased earlier in autumn than the other ChlF variables. This was likely associated with the decline in incoming radiation. The simulated GPP was a good match with observations during autumn. The simulated $\Phi_{f,s}$ declined simultaneously with the observed ChlF variables, however, from November to beginning of February it was on a lower level compared to them. This might be connected to the way electron transport rate (ETR) was simulated in the model. In the Farquhar model the temperature dependency of the parameter has a lot of influence on ETR, whereas the observed ChlF variables gave reason to suggest that the ETR stayed on a higher level later to the winter. The gradual decline of the observed ChlF variables might be due to dark autumns, as the needles do not suffer from excess light levels and thus the downregulation of the light harvesting machinery can be much lower (Kolari et al., 2014). The yield of photochemistry and fluorescence declines during winter because the yield of NPQ increased in a process regulated by air temperature (Porcar-Castell, 2011).

The observed ChlF variables drop to their lowest value in February and March. This was the time period, when the forest was experiencing stress because of the increasing light levels, but still persisting soil freeze and low air temperatures. The trees will have need for photoprotection in order to get rid of the excess light energy that they cannot yet use for photosynthesis, because of the prevailing conditions. Therefore the observed ChlF values obtained their lowest values in this time period. The low values in the simulated ChlF variables are caused only by low temperatures, the mechanisms related to photoprotection are not included in the current model implementation.

Simulated $\Phi_{f,sp}$ showed an earlier ascent in spring, and this was connected to simulated photosynthesis that commenced too early, clearly seen in the half-hourly GPP values in Fig. 1b. The comparison between simulated $\Phi_{f,sp}$, SIF and observed incoming PAR showed that in spring $\Phi_{f,sp}$ that slowed down the increase of SIF to its summertime values, whereas in autumn light limitation caused the withdrawal of SIF (Supplement A, Fig. A1).

Some negative GPP values are present in Fig. 1. The random nature of turbulence and instrument uncertainty add to measurement uncertainty (Rannik et al., 2016). The GPP is obtained from the observed net ecosystem exchange (NEE) by subtracting the respiration that has been estimated by a regression fit to temperature (Wohlfahrt and Galvano, 2017). Thus the random measurement error leads to some negative GPP values that are compensated by equal amount of too high positive values, additionally the temperature fit to respiration causes some systematic error in the values.

Observed F’ and Φ_p decreased at high light levels (known as mid-day depression) on a sunny day (Supplement A, Fig. A2). While this decline also occured in simulated $\Phi_{f,s}$, simulated SIF is increased with incoming radiation. On a cloudy day, observed F’ increased during the day, whereas Φ_p showed some decrease from the morning value (Supplement A, Fig. A3). Simulated $\Phi_{f,s}$ and SIF both increased during daytime under favorable photosynthesis conditions. This is in agreement with the expected inverse relationship between Φ_f and Φ_p under low light conditions and the positively correlated relationship under high light conditions.

3.2 Upscaling to site scale

In JSBACH, most of the ChlF signal originated from the top of the canopy, as it received most of the light and, therefore, the largest part of photosynthesis takes place here (Fig. 2). On a sunny day around midday, 86% of total canopy GPP and 88% of SIF was produced in the uppermost layer. On a cloudy day 97% of the total canopy GPP and 98% of the total canopy SIF was generated in the uppermost layer.

3.3 Comparison of remote sensing results at site scale

Overall, the remotely sensed SIF signal followed the seasonal cycle of observed GPP and modelled SIF and GPP at the flux sites (Fig. 3). Observed and modelled SIF showed a larger correlation to observed and modelled GPP, respectively, than fAPAR, in particular the FI-Hyy and FI-Ken sites (Table 2). The model was better at predicting the observed GPP than observed SIF (Table 2), which might reflect the scale mismatch of the SIF observations. Nevertheless, the ability of JSBACH to simulate fAPAR was not as good as its simulation of the SIF signal (Table 2).

The correlation between observed SIF and observed GPP was higher at the southern sites than at the northern sites (Table 2). This was related to the observed early spring behavior SIF signal in February that took place before photosynthesis occurred in the simulations or observations (Fig. 3). During late winter and spring the observed SIF signal reached 40% of the summertime maximum value at the northern sites, which cannot be explained by environmental conditions. Early increases in observed SIF also occurred at the two southern sites, but were not as pronounced as at the northern sites in relative terms, as the northern sites had lower values of SIF overall. After this early increase, the signal lowered again. Further investigations of the SCIAMACHY observations showed that the same phenomena also took place at FI-Ken (see Supplementary Material B).

The modelled GPP had the tendency to increase too early in spring, which was clearly seen at FI-Kns (Fig. 3a) and FI-Sod (Fig. 3e). This increase happened shortly before the start of the observed photosynthesis. This early emergence of photosynthesis contributed to the inability to simulate the observed SIF signal.

The slope between modelled GPP and SIF was 8.7 g C m^{-2} day^{-1}/(unitless) (standard deviation 0.5 g C m^{-2} day^{-1}/unitless) averaged over the four sites (Table 3). It is close to the slope between observed GPP and SIF averaged over the four sites, which was 8.9 g C m^{-2} day^{-1}/ mW m^{-2} sr^{-1} nm^{-1}(standard deviation 1.0 g C m^{-2} day^{-1}/ mW m^{-2} sr^{-1} nm^{-1}). The slopes of the regressions between GPP and SIF were reasonably similar between

~~simulations and observations across the different sites (Table 3).~~ Despite this similarity of averaged values, the slopes between the model and simulations were not within the uncertainty at any other site than FI-Hyy and their results are not directly comparable, as the units are different. However, the standard deviations were lower for GPP vs. SIF fits than for fAPAR fits, when compared to the absolute values of the slopes. ~~This was in contrast to~~ T~~t~~he slope between GPP and fAPAR in the observations~~, which~~ was higher for the southern sites compared to the northern sites and the same was observed for the modelled slopes. The differing slopes between simulations and observations for the GPP vs. fAPAR fits resulted from differing ranges in the simulated and observed fAPAR values. The southern sites had higher GPP vs. fAPAR slopes, since the GPP values at the southern sites had much higher summertime values than the northern sites, although the fAPAR values showed a similar range at all the sites.

3.3.1 Year 2009 at FI-Ken

Modelled GPP and modelled SIF were well correlated with each other at all sites except FI-Ken (Table 2), which showed decoupling of these two variables in summer 2009 (Fig. 3g). In contrast to the observations, the model predicted a drought-related decline in summertime GPP in 2009. This might be due to the presence of a thin ~~peat~~ humus layer at FI-Ken, which probably makes the site more resistant to drought (Hillel, 1980), whereas JSBACH is only able to simulate freely draining upland soils.

The ensuing decoupling of modelled SIF and GPP variables was connected to the current formulation of the actual electron transport rate (J_a) in the model (eq. (A6)). The formulation of eq. (A6) states that the actual electron transport rate is J from eq. (2) when photosynthesis is limited by the electron transport rate.

At FI-Ken the simulated summer drought influenced the simulated GPP via soil moisture limitation in the stomatal conductance. In the JSBACH model, soil moisture limitation causes a reduction in both the electron transport and the carboxylation rate limited branches of photosynthesis. This is different from other models, such as SCOPE, in which drought causes an additional decrease in $V_{c(max)}$ that further drives down the carboxylation rate limited carbon assimilation A_c and results in a shift to carboxylation rate limited photosynthesis. Closer examination of the FI-Ken simulation results revealed that it was mostly dominated by the electron transport rate limited photosynthesis, therefore the drought effect seen in simulated GPP did not lower SIF.

3.4 Regional runs

The correlation between observed and simulated SIF for the averaged five year period was reasonably high (r^2=0.86~~0~~) for different grid points in the study region~~, with the largest deviations between the two sites in the high latitude regions~~. The correlation between simulated GPP values and the MPI-BGC GPP product was at a similar level (r^2=0.78). Overall, simulated GPP values were lower than the estimates from the data-driven MPI-BGC GPP, with the highest simulated GPP values less than 1200 g C m^{-2} $year^{-1}$ while most of the grid points located south of 58°N according to the MPI-BGC GPP have larger values. The distribution of GPP on the map showed that the MPI-BGC GPP-product predicts much larger GPP values for the Norwegian coast than JSBACH (Fig. 4). During winter months, larger GPP values than in the surrounding regions were also seen in the MPI-BGC product (Fig. 4p). The low values in that region in JSBACH originated from the vegetation maps used for the generation of the PFT distribution. A pronounced difference between the model results and observations is that the simulated GPP ~~and SIF~~ reached the zero level, whereas this did~~oes~~ not occur for the ~~observed SIF or~~ MPI-BGC GPP-product, which was not below 380 g C m^{-2} $year^{-1}$ in our study region.

Modelled GPP and MPI-BGC GPP-product showed a similar pattern as the observed and modelled SIF along a longitudinal transect at 28°E with little difference in elevation (Fig. 5). At lower latitudes, MPI-BGC GPP was lower, which was not evident in the modelled ~~other~~ variables. The observed SIF had maximum at higher latitude than other shown variables and shows therefore also lower level in high latitude values. At high latitudes (> 69.5°), the estimates from JSBACH dropped noticeably compared to the ~~observed SIF and~~ MPI-BGC GPP product.

During spring, satellite observed SIF showed a number of larger values in central Finland (Fig. 4a) that were not seen in the model variables (Fig. 4b-d). In summer, satellite observed SIF showed a larger gradient in the north-south direction than the model variables (Fig. 4e-h). This might reflect the fact that the observed gradient in green biomass was larger than seen in the simulations (Markkanen et al., in preparation). In autumn, the geographical distribution was quite similar between observed and modelled SIF and GPP variables (Fig. 4i-l). This might be connected to the strong light dependence of SIF and GPP, both in real world and simulations, as light is a very important driver for photosynthesis in autumn. At winter, satellite observed SIF showed some scattering in the area where it had values (Fig. 4m). These values were likely connected to the challenges of winter time measurements (e.g. low light levels) with GOME-2.

At the seasonal scale, the strongest correlation (r^2=0.87) between satellite observed and simulated SIF occurred in autumn (September-November) (Fig. 6c). The high correlation during autumn is likely related to the inherent light dependency of both GPP and SIF as light diminishes along latitudinal gradient. The slope of the fit between observed and modelled SIF values changed ~~notably~~ in spring compared to the summer and autumn periods. This was caused by our large latitudinal gradient of the region. In the southernmost region there appears to be some linear dependency between modelled and observed SIF, but in the northernmost region the modelled SIF values are still very close to zero. ~~a more narrow range in the observed values, even though more light was available during the spring period (March-May) compared to the autumn period~~

~~(September-November) in our classification of seasons. There was also some change in the actual overpass time of GOME-2 that occurred between mid-summer and the other seasons and this also might have influenced the results.~~

The seasonal cycle at a monthly resolution for the different latitudinal regions revealed differences between the modelled and observed SIF (Fig. 7a). The highest SIF in the simulations occurred in July in all latitudinal regions. However, the highest value in the observations in low latitude regions occurred in June while in region 62-66°N highest value took place in July and ~~s~~ north of 66°N the highest value occurred in August. Two of the studied micrometeorological measurement sites were located in the northernmost latitudinal region. At FI-Ken, observed SIF predicted the highest activity one month later than the observed GPP. ~~Moreover, the early increase of SIF in late winter, which was evident at the site level in the northern sites, was visible in this seasonal cycle. This phenomenon was also visible in the SCIAMACHY and OCO-2 results (see Supplementary Material B).~~ As with simulated SIF, simulated GPP from JSBACH showed the highest value in July, even though in the two most southern regions June and July were at a similar level (Fig. 7b). The highest values of GPP in Denmark occur in June due to the cultured crops (Lansø, 2016) and similar crops might also influence seasonal cycle in the Baltic region. The GPP from MPI-BGC was similar to the satellite observed SIF highest value in the southernmost region in June and for the other regions the highest values occurred in July (Fig. 7b).

4 Discussion

4.1 Site level observations

The implementation of the SIF leaf-scale model into JSBACH performed appropriately when compared to observations from FI-Hyy, a typical coniferous site for southern Finland. The fact that both simulated GPP and ChlF increased earlier than their observed counterparts in spring would suggest that ChlF observations might be successful in improving modelling of photosynthesis, e.g., in a data assimilation set-up (Koffi et al., 2014; Norton et al., 2017). ~~The premature increase in simulated GPP in spring may have been caused by the static temperature responses of photosynthesis parameters implemented in JSBACH, even though studies using field data suggest seasonal acclimation of these parameters (Thum et al., 2008; Kolari et al., 2014). Moreover, the effect of frost on stomatal conductance, not included in the model, might also be important.~~ However, it should also be noted, that the data for FI-Hyy was derived from active measurements, and that the coupling between Φ_p and Φ_f might be changed during different seasons (Krivosheeva et al., 1996). Active measurements have different variables than the “passive” quantities obtained from the model, and therefore, there is reason to be cautious with the comparison.

The SIF and fAPAR are close to each other in observations, as they are both related to green biomass. However, in the JSBACH model their calculation is different with fAPAR derived as a function of LAI and radiation, whereas GPP (and therefore SIF) is a function of other environmental variables and model parameters (in addition to LAI and radiation) that may also have an effect.

In spring all studied ChlF variables increased simultaneously with photosynthesis. However, in autumn, the decline in Φ_p was much slower than in F'. This slow decline might be due to dark autumns, as the needles do not suffer from excess light levels and thus the downregulation of the light harvesting machinery can be much lower (Kolari et al., 2014). The yield of photochemistry and fluorescence declines during winter because the yield of NPQ increased in a process regulated by air temperature (Porcar-Castell, 2011). Therefore, the needles will be more protected against high light levels during the spring when the air temperature remains low and photosynthesis is curbed.

The photosynthesis of forests is often modelled using constant temperature response for the biochemical model parameters V_{max} and J_{max} throughout the year. However, studies have revealed that this assumption does not hold for ecosystems with strong seasonal cycles, but causes overestimation of CO_2 fluxes in transition periods, at least in spring. Kolari et al. (2014) found seasonally varying values for leaf level for those parameters from leaf level observations at FI-Hyy. Ueyama et al. (2016) found seasonally varying biochemical model values at four different black spruce forests in Alaska in a model inversion study at eddy covariance sites. In an earlier study using inversion at boreal coniferous forests (Thum et al., 2008), it was found that three forests at northern boreal zone (FI-Hyy, FI-Sod and FI-Ken) had temporal evolution in the biochemical parameters, but a site located on temperate boreal (Norunda, Sweden) did not.

Leaf level studies have used temperature acclimation for the changes of biochemical parameters (Wang et al., 1996). Similar results have been obtained for site level results at FI-Sod, where dark acclimated chlorophyll fluorescence observations have been used in combination with eddy covariance observations to disentangle the effect of changing maximum photosynthetic capacity (Thum et al., 2017).

The changes taking place in the needles of conifer forests in winter are numerous to protect the needles in challenging environmental conditions. E.g. the light harvesting complexes are aggregated (Porcar-Castell, 2011) and the xanthophyll cycle enables photoprotection (Ensminger et al., 2004). Some of these processes can be in future be included in a large scale model, as adding changes to the parameters in the ChlF model discussed below, but as changes in the boreal spring happen at quite fast pace and those can be tracked with several different environmental and biological variables (Thum et al., 2009), for large scale applications a temperature related changing of the biochemical parameters might be next step forward and remotely sensed SIF observations provide a very useful evaluation tool in this context."

In addition, tThe number of active PSII reaction centers (parameter q_{Ls} in the chlorophyll fluorescence model) has been shown to change seasonally in boreal environments (Porcar-Castell, 2011). However, in our implementation we assumed it to be a constant 0.5, as there is no theory to predict variations of this parameter at larger scales. Similarly the rate constant of sustained thermal dissipation (parameter k_{NPQs} in the chlorophyll fluorescence model) incorporates seasonal variation in boreal forests (Porcar-Castell, 2011), but for the same reasons it was kept as zero in our model runs. The comparison with the data nevertheless suggests that these assumptions are justified at the time and spatial scales of our analysis.

However, since the seasonal cycle was captured quite well by the model at FI-Hyy, even though the seasonally variable parameters that control yield were not considered, some concerns connected with the model are evident. The link to the Farquhar model causes the simulated ChlF variables to have a pronounced seasonal cycle similar to the measurements, even though the light reactions of the SIF model do not include the seasonal changes that take place in the leaves. While this could be considered as a counterargument against our approach, the fact that we can generate an appropriate time series with the environmental controls of the Farquhar model suggests that our approach maybe a sensible choice when attempting to simulate SIF at ecosystem and larger scales.

4.2 Satellite data

The satellite SIF observations have a clear-sky bias, which may affect the seasonality of these data. Furthermore, illumination and viewing geometries affect the observed SIF (Joiner et al., 2013). The high wintertime values observed by GOME-2 for SIF at the Finnish sites were not likely connected to photosynthetic activity and they were also below the error threshold of the observations. It is likely that this would be more visible in the northern sites, where SIF values are generally lower. During winter there are some warm days when the forests might be active, although the activity is not as comparable in magnitude to the summer time as these values would suggest. The phenomenon is not connected to snow reflectance as SIF measures emissions only from the green component of the canopy. Similar behavior has been observed at some other boreal forest regions in GOME-2 data, but it is not common in the boreal region (Walther et al., 2016). Moreover, this was also noticed in the SCIAMACHY and OCO-2 data (Supplementary Material, B). These characteristics would indicate that care must be taken when SIF data is used for evaluation of modelled photosynthesis or in data assimilation in boreal regions. Also, the low SIF values measured at high latitudes make the data over those regions prone to systematic errors, which may affect the consistency of the time series. In addition, the illumination-observation geometry might play a role in canopy structure effects and its seasonality.

Here we compared site level observations with satellite observations, despite the fact that these two observations are at completely different spatial scales. A flux tower measures approximately 1 km^2 of the surrounding area, whereas the satellite observations have a wider footprint (e.g.

for GOME-2 default footprint is 80 km x 40 km). However, Finnish territory consists of large areas of forest and the seasonal cycle is driven by meteorological variations that have an influence at larger spatial scales, and therefore we consider the comparison between these different scales to be appropriate assuming a homogeneous landscape.

At large scale the ability of SIF to estimate the seasonal cycle of GPP has been shown at boreal coniferous forests (Walther et al., 2016). At the leaf scale the connection is more complex. The seasonal dynamics of interplay between ChlF and photosynthesis still remain unclear, and a model that captures that relationship is not currently available (Porcar-Castell et al., 2014). If alternative electron sinks or metabolic pathways exist, as was found by Krivosheeva et al. (1996) for wintering Scots pines, then this may mean that the use of ChlF as a proxy for seasonal dynamics of GPP is problematic (Porcar-Castell et al., 2014). Development of process-based models for ChlF is ongoing and once a suitable leaf-level model that incorporates the seasonal changes in the ChlF becomes available, then it could be used to parameterize the larger scale models.

4.3 Challenges in modelling: Radiative transfer

A significant challenge to the comparison of modelled and observed SIF is the radiative transfer in the canopy. However, as most of the detectable ChlF signal originates from the topmost canopy layer (van der Tol et al., 2014), a complicated radiative transfer scheme is not essential for a first order comparison that focuses on the seasonal cycle and large-scale gradients. This assumption is consistent with our model, which predicts that the largest part of the SIF signal originates from the topmost layer of the canopy. Therefore, we would suggest that our simplifications in treating the radiative transfer of SIF in the canopy are adequate for the purpose of this study.

5 Conclusions

SIF in a northern coniferous forest occurred simultaneously with GPP in both observations and simulations across Finland and the Fenno-Scandinavian region. Site level comparisons to flux tower observations of GPP support these results. The leaf level measurements provided the first comparison to simulations and it is also essential that site-level SIF observations are available, such as in study by Yang et al. (2015). A measurement set-up is currently being tested at FI-Sod that will also provide data suitable for modelling purposes.

The main findings of our study include:

- JSBACH was better in simulation of SIF than fAPAR at the site scale.

- Observed SIF was better at capturing the seasonal cycle at the forest sites than the modelled SIF and GPP, therefore it can be used to constrain modelled SIF in order to improve the simulated GPP.
- Correlation between observed SIF and observed GPP was higher in the southern than in the northern sites.
- Slopes of regression between GPP and SIF were similar between simulations and observations across different sites.
- Slopes of regression between observed GPP and fAPAR were higher in the southern than in the northern sites, and the same trend occurred for the simulated values.
- Satellite observed SIF showed a maximum seasonal value in July for the area north of latitude 66°, in contrast to the simulated SIF and simulated and observed GPP values.

Further evaluation of these results would benefit from the additional use of other remote sensing products for LAI estimates, as LAI has a strong influence on the spatial variation of the SIF signal. Current and future space missions (e.g. Guanter et al., 2014) as well as increased ground and airborne SIF observations will further provide data to relate SIF to photosynthesis.

6 Code availability

The SCOPE model is available from Christiaan Van Der Tol. The chlorophyll fluorescence model is available from Federico Magnani. The JSBACH model is available to the scientific community under a version of the Max Planck Institute for Meteorology Software License Agreement (http://www.mpimet.mpg.de/en/science/models/license/).JSBACH is property of the Max Planck Institute.

7 Data availability

The leaf level chlorophyll fluorescence data is available from Albert Porcar-Castell and will be available from http://avaa.tdata.fi/web/smart/smear during winter 2016-2017. The micrometeorological data and meteorological data is available from Annalea Lohila (FI-Kns), Mika Aurela (FI-Ken and FI-Sod) and at http://avaa.tdata.fi/openida/dl.jsp?pid=urn:nbn:fi:csc-ida-2x201611242015017385197s for FI-Hyy.

8 Appendices

Appendix A: Leaf-level chlorophyll fluorescence model

The leaf level model for ChlF is based on work by Magnani and Dayyoub (2016). The definitions of the variables and parameters and their possible numerical values and references are in Table A1.

Excitation energy that enters the leaf will be dissipated through photochemistry (subscript *p*), fluorescence (*f*), energy-independent (*D*) and energy-dependent heat dissipation (*NPQ*) with the following yields (Φ) calculated with rate constants k_i:

$$\Phi_p = \frac{k_p}{k_p+k_f+k_D+k_{NPQ}} \qquad \text{(A1a)}$$

$$\Phi_f = \frac{k_f}{k_p+k_f+k_D+k_{NPQ}} \qquad \text{(A1b)}$$

$$\Phi_D = \frac{k_D}{k_p+k_f+k_D+k_{NPQ}} \qquad \text{(A1c)}$$

$$\Phi_{NPQ} = \frac{k_{NPQ}}{k_p+k_f+k_D+k_{NPQ}} \qquad \text{(A1d)}$$

The rate constant of photochemistry (k_p) can be expressed as a function of the intrinsic rate of photochemistry (k_{PSII}), photochemical quenching parameter qL_T (representing the fraction of functional and open reaction centers) consisting of qL_r (the fraction of open reaction centers) and qL_s (the fraction of functional reaction centers, the sustained component of the photochemical quenching parameter):

$$k_p = k_{PSII} \cdot qL_T = k_{PSII} \cdot qL_s \cdot qL_r \qquad \text{(A2)}$$

The rate constant for regulated thermal energy dissipation (k_{NPQ}) consists of reversible component (*NPQs*) and sustained component (*NPQr*):

$$k_{NPQ} = k_{NPQs} + k_{NPQr} \qquad \text{(A3)}$$

The fluorescence and photochemistry yields can be expressed by combining equations (A1-4):

$$\Phi_p = \frac{k_{PSII} \cdot qL_s \cdot qL_r}{k_{PSII} \cdot qL_s \cdot qL_r + k_f + k_D + k_{NPQr} + k_{NPQs}} \quad \text{(A4a)}$$

$$\Phi_f = \frac{k_f}{k_{PSII} \cdot qL_s \cdot qL_r + k_f + k_D + k_{NPQr} + k_{NPQs}} \quad \text{(A4b)}$$

and the ratio of these two gives:

$$\frac{\Phi_p}{\Phi_f} = \frac{k_{PSII}}{k_f} \cdot qL_s \cdot qL_r \quad \text{(A5)}$$

The actual electron transport J_a is

$$J_a = J(I) \cdot \frac{A}{A_j} \quad \text{(A6)}$$

where A is photosynthesis (minimum of the electron transport rate limited photosynthesis A_j,and maximum carboxylation rate limited photosynthesis, A_c, in units μmol m^{-2} s^{-1}), J is the electron transport shown in eq. (2). The J_a is used in the calculation to describe the fraction of incoming quanta that is used for photosynthesis, i.e. the photochemical quantum yield of photosystem II (PSII), Φ_p

$$\Phi_p = \frac{J_a}{I} \quad \text{(A7)}$$

The rate of PSII reduction can be assumed to be proportional to the fraction of functional and closed reaction centers:

$$J_a = qL_s \cdot (1 - qL_r) \cdot J_{max} \quad \text{(A8)}$$

Therefore, the fraction of reaction centers that are functional and open is:

$$qL_s \cdot qL_r = qL_s - \frac{I \cdot \Phi_p}{J_{max}} \quad \text{(A9)}$$

By substituting eq. (A9) to eq. (A5), the following expression for fluorescence yield is obtained:

$$\Phi_{f,1} = \Phi_p \cdot \frac{k_f}{k_{PSII}} \cdot \frac{1}{qL_s - \frac{I \cdot \Phi_p}{Jmax}} \qquad (A10)$$

The rate constant k_{NPQ} is constant or close to zero in conditions of light-limited carboxylation (Walters et al., 1993), as energy dependent heat dissipation is the result of pH build-up in the thylakoid lumen and xanthophyll de-epoxidation. From eq. (A1b) and (A1d) the thermal energy dissipation in low light conditions is:

$$\Phi_{NPQ} = \Phi_f \cdot \frac{k_{NPQs}}{k_f} \qquad (A11)$$

From eq. (A1b) and (A1c) we obtain:

$$\Phi_D = \Phi_f \frac{k_D}{k_f} \qquad (A12)$$

Under these conditions a negative relationship between photochemical and fluorescence yields is expected, since:

$$\Phi_p = 1 - \Phi_f - \Phi_D - \Phi_{NPQ} = 1 - \Phi_f - \Phi_f \cdot \frac{k_D}{k_f} - \Phi_f \frac{k_{NPQs}}{k_f} \qquad (A13)$$

From this equation fluorescence yield at low light conditions can be derived to be:

$$\Phi_{f,2} = (1 - \Phi_p) \cdot \left(\frac{k_f}{k_f + k_D + k_{NPQs}}\right) \qquad (A14)$$

The fluorescence yield of PSII, Φ_f, is taken as the minimum of $\Phi_{f,1}$ and $\Phi_{f,2}$:

$$\Phi_f = \min(\Phi_{f,1}, \Phi_{f,2}) \qquad (A15)$$

The reference minimum fluorescence yield, obtained in dark-acclimated foliage in the absence of stress $\Phi_{f,0}$ can be theoretically derived from the rate constant of fluorescence k_f ($6.7 \cdot 10^7$ s^{-1}) (Rabinowich and Govindjee, 1969), the rate constant of thermal deactivation k_D ($6.03 \cdot 10^8$ s^{-1}) and the rate constant for photochemistry in open PSII reaction centers k_{PSII} as

$$\Phi_{f,0} = \frac{k_f}{k_f + k_{PSII} + k_D} \quad \text{(A16)}$$

and k_{PSII} (Genty et al., 1989) can be derived as

$$k_{PSII} = \frac{(k_D + k_f) \cdot \Phi_{p,max}}{(1 - \Phi_{p,max})} \quad \text{(A17)}$$

where $\Phi_{p,max}$ (0.88 mol / E) is the maximum quantum yield of PSII in dark-acclimated conditions in the absence of stress obtained fluorometrically after correction for PSI fluorescence (Pfundel, 1998).

To obtain the scaled fluorescence yield $\Phi_{f,s}$, the fluorescence yield Φ_f is further divided by $\Phi_{f,0}$,

$$\Phi_{f,s} = \frac{\Phi_f}{\Phi_{f,0}} \quad \text{(A18)}$$

9 Author contribution

T. Thum and S. Zaehle did the implementation of the chlorophyll fluorescence model into the JSBACH model. P. Köhler and L. Guanter provided remote sensing data. M. Aurela and T. Laurila provided the micrometeorological and meteorological data for sites FI-Ken and FI-Sod. A. Lohila provided data for FI-Kns and P. Kolari for FI-Hyy. F. Magnani contributed the chlorophyll fluorescence model and C. Van Der Tol the SCOPE model. T. Markkanen set-up the regional model and prepared the meteorological forcing data for the model. T. Thum did the simulations and analyzed the data with help of the co-authors. T. Thum prepared the manuscript with contributions from all co-authors.

10 Competing interests

Author S. Zaehle is a member of the editorial board of the journal.

11 Acknowledgements

TT acknowledges funding from the Academy of Finland (grant number 266803). We thank Dr. Thomas Kaminski for providing fAPAR data for all the regions and sites. Help from Dr. Leif Backman in acquisition of ERA-Interim data is acknowledged. We thank the Academy of Finland Centre of Excellence (grant no. 1118615 and 272041). We thank Dr. Martin Jung for the use of the MPI-BGC GPP product. We are grateful to Dr. Albert Porcar-Castell for sharing his leaf-level ChlF data from Hyytiälä and for fruitful discussions. We thank Sophia Walther and Kristin Böttcher for their valuable comments on the manuscript. Two anonymous referees whose comments greatly improved the manuscript are gratefully acknowledged.

12 References

Aurela M., Lohila A., Tuovinen J.-P., Hatakka J., Penttilä T. and Laurila, T.: Carbon dioxide and energy flux measurements in four northern-boreal ecosystems at Pallas, Boreal Env. Res., 20, 455–473, 2015.

Baker, N. R.: Chlorophyll fluorescence: A probe of photosynthesis in vivo, Annual Review of Plant Biology, 59, 89-113, 2008.

Bergh, J., McMurtrie, R. E., and Linder, S.: Climatic factors controlling the productivity of Norway spruce: a model-based analysis, Forest Ecol. Manag., 110, 127–139, 1998.

Bonan, G.B.: Forests and climate change: Forcings, feedbacks, and the climate benefits of forests, Science, 320, 1444–1449, 2008.

Böttcher K., Aurela, M., Kervinen, M., Markkanen, T., Mattila, O.-P., Kolari, P., Metsämäki, S., Aalto, T., Arslan, A. and Pulliainen, J.: MODIS time-series-derived indicators for the beginning of the growing season in boreal coniferous forest - A comparison with CO_2 flux measurements and phenological observations in Finland, Remote Sens. Environ., 140, 625-638, 2014.

Collatz, G. J., Ribas-Carbo, M., and Berry, J. A.: Coupled photosynthesis-stomatal conductance model for leaves of C4 plants, Aust. J. Plant Physiol., 19, 519–538, doi:10.1071/PP9920519, 1992.

Dee, D. P., Uppala, S. M., Simmons, A. J., Berrisford, P., Poli, P., Kobayashi, S., Andrae, U., Balmaseda, M. A., Balsamo, G., Bauer, P., Bechtold, P., Beljaars, A. C. M., van de Berg, L., Bidlot, J., Bormann, N., Delsol, C., Dragani, R., Fuentes, M., Geer, A. J., Haimberger, L., Healy, S. B., Hersbach, H., Hólm, E. V., Isaksen, L., Kållberg, P., Köhler, M., Matricardi, M., McNally, A. P., Monge-Sanz, B. M., Morcrette, J.-

J., Park, B.-K., Peubey, C., de Rosnay, P., Tavolato, C., Thépaut, J.-N., and Vitart, F.: The ERA-Interim reanalysis: configuration and performance of the data assimilation system, Q.J.R. Meteorol. Soc., 137, 553–597, 2011.

Dickinson, R. E.: Land surface processes and climate-surface albedos and energy balance, Adv. Geophys., 25, 305–353, 1983.

Farquhar G.D., von Caemmerer S., and Berry J.A.: A biogeochemical model of photosynthesis in leaves of C3 species, Planta, 149, 78–90, 1980.

Frankenberg, C., Fisher, J. B., Worden, J., Badgley, G., Saatchi, S. S., Lee, J.-E., Toon, G. C., Butz, A., Jung, M., Kuze, A., and Yokota, T.: New global observations of the terrestrial carbon cycle from GOSAT: Patterns of plant fluorescence with gross primary productivity, Geophys. Res. Lett., 38, L17706, doi:10.1029/2011GL048738, 2011.

Frankenberg, C., O'Dell, C., Berry, J., Guanter, L., Joiner, J., Köhler, P., Pollock, R., and Taylor, T. E.:. Prospects for chlorophyll fluorescence remote sensing from the Orbiting Carbon Observatory-2, Remote Sens. Environ., 147, 1–12, 2014.

Giorgetta M. A., Jungclaus, J., Reick, C. H., Legutke, S., Bader, J., Böttinger, M., Brovkin, V., Crueger, T., Esch, M., Fieg, K., Glushak, K., Gayler, V., Haak, H., Hollweg, H.-D., Ilyina, T., Kinne, S., Kornblueh, L., Matei, D., Mauritsen, T., Mikolajewicz, U., Mueller, W., Notz, D., Pithan, F., Raddatz, T., Rast, S., Redler, R., Roeckner, E., Schmidt, H., Schnur, R., Segschneider, J., Six, K. D., Stockhause, M., Timmreck, C., Wegner, J., Widmann, H., Wieners, K.-H., Claussen, M., Marotzke, J., and Stevens, B.: Climate and carbon cycle changes from 1850 to 2100 in MPI-ESM simulations for the Coupled Model Intercomparison Project phase 5, J. Adv. Model. Earth Syst., 5, 572–597, 2013.

Guanter, L., Aben, I., Tol, P., Krijger, J. M., Hollstein, A., Köhler, P., Damm, A., Joiner, J., Frankenberg, C., and Landgraf, J.: Potential of the TROPOspheric Monitoring Instrument (TROPOMI) onboard the Sentinel-5 Precursor for the monitoring of terrestrial chlorophyll fluorescence, Atmos. Meas. Tech., 8, 1337–1352, 2015.

Guanter, L., Frankenberg, C., Dudhia, A., Lewis, P. E., Gómez-Dans, J., Kuze, A., Suto, H., and Grainger, R. G.: Retrieval and global assessment of terrestrial chlorophyll fluorescence from GOSAT space measurements, Remote Sens. Environ., 121, 236–251, dx.doi.org/10.1016/j.rse.2012.02.006, 2012.

Hillel, D.: Fundamentals of Soil Physics, Academic Press, 413 pp., 1980.

Jacob, D., and Podzun, R.: Sensitivity studies with the regional climate model REMO, Meteorol. Atmos. Phys., 63, 119–129, 1997.

Jacob, D.,: A note to the simulation of the annual and inter-annual variability of the water budget over the Baltic Sea drainage basin, Meteorol. Atmos. Phys., 77, 61–73, 2001.

Jacob, D., Van den Hurk, B. J. J. M., Andrae, U., Elgered, G., Fortelius, C., Graham, L. P., Jackson, S. D., Karstens, U., Köpken, Chr., Lindau, R., Podzun, R., Rockel, B., Rubel, F., Sass, B. H., Smith, R. N. B., and Yang, X.: A comprehensive model inter-comparison study investigating the water budget during the BALTEX-PIDCAP period, Meteorol. Atmos. Phys., 77, 19–43, 2001.

Joiner, J., Guanter, L., Lindstrot, R., Voigt, M., Vasilkov, A. P., Middleton, E. M., Huemmrich, K. F., Yoshida, Y., and Frankenberg, C.: Global monitoring of terrestrial chlorophyll fluorescence from moderate-spectral-resolution near-infrared satellite measurements: methodology, simulations, and application to GOME-2, Atmos. Meas. Tech., 6, 2803-2823, doi:10.5194/amt-6-2803-2013, 2013.

Joiner, J., Yoshida, Y., Vasilkov, A. P., Middleton, E. M., Campbell, P. K. E., Yoshida, Y., Kuze, A., and Corp, L. A.: Filling-in of near-infrared solar lines by terrestrial fluorescence and other geophysical effects: simulations and space-based observations from SCIAMACHY and GOSAT, Atmos. Meas. Tech., 5, 809-829, doi:10.5194/amt-5-809-2012, 2012.

Joiner, J., Yoshida, Y., Vasilkov, A.P., Schaefer, K., Jung, M., Guanter, L., Zhang, Y., Garrity, S., Middleton, E.M., Huemmrich, K.F., Gu, L., and Belelli Marchesini, L.: The seasonal cycle of satellite chlorophyll fluorescence observations and its relationship to vegetation phenology and ecosystem atmosphere carbon exchange, Remote Sens. Environ., 152, 375-391, dx.doi.org/10.1016/j.rse.2014.06.022, 2014.

Joiner, J., Yoshida, Y., Vasilkov, A. P., Yoshida, Y., Corp, L. A., and Middleton, E. M.: First observations of global and seasonal terrestrial chlorophyll fluorescence from space, Biogeosciences, 8, 637-651, doi:10.5194/bg-8-637-2011, 2011.

Jung, M., Reichstein, M., and Bondeau, A.: Towards global empirical upscaling of FLUXNET eddy covariance observations: validation of a model tree ensemble approach using a biosphere model, Biogeosciences, 6, 2001-2013, doi:10.5194/bg-6-2001-2009, 2009.

Jung, M., Reichstein, M., Margolis, H. A., Cescatti, A., Richardson, A. D., Arain, M. A., Arneth, A., Bernhofer, C., Bonal, D., Chen, J. Gianelle, D., Gobron, N., Kiely, G., Kutsch, W., Lasslop, G., Law, B. E., Lindroth, A., Merbold, L., Montagnani, L., Moors, E. J., Papale, D., Sottocornola, M., Vaccari, F., and Williams, C.: Global patterns of land-atmosphere fluxes of carbon dioxide, latent heat, and sensible heat derived from eddy covariance, satellite, and meteorological observations, J. Geophys. Res., 116, G00J07, doi:10.1029/2010JG001566, 2011.

Koffi, E. N., Rayner, P. J., Norton, A. J., Frankenberg, C., and Scholze, M.: Investigating the usefulness of satellite derived fluorescence data in inferring gross primary productivity within the carbon cycle data assimilation system, Biogeosciences 12, 4067-4084, doi:10.5194/bg-12-4067-2015.

Köhler, P., Guanter, L., and Joiner, J.: A linear method for the retrieval of sun-induced chlorophyll fluorescence from GOME-2 and SCIAMACHY data, Atmos. Meas. Tech., 8, 2589-2608, doi:10.5194/amt-8-2589-2015, 2015.

Kolari, P., Chan, T., Porcar-Castell, A., Bäck, J., Nikinmaa, E. and Juurola, E.: Field and controlled environment measurements show strong seasonal acclimation in photosynthesis and respiration potential in boreal Scots pine, Front. Plant Sci., 5, 717, doi: 10.3389/fpls.2014.00717, 2014.

Kolari, P., Kulmala, L., Pumpanen, J., Launiainen, S., Ilvesniemi, H., Hari, P. and Nikinmaa, E.: CO_2 exchange and component CO_2 fluxes of a boreal Scots pine forest, Boreal Environ. Res., 14, 761-783, 2009.

Knorr, W.: Annual and interannual CO_2 exchanges of the terrestrial biosphere: process-based simulations and uncertainties, Global Ecol. Biogeogr., 9, 225-252, 2000.

Krivosheeva, A., Tao, D. L., Ottander, C., Wingsle, G., Dube, S. L., Öquist, G.: Cold acclimation and photoinhibition of photosynthesis in Scots pine, Planta, 200, 296-305, 1996.

Lansø, A. S.: Mesoscale modelling of atmospheric CO_2 across Denmark, PhD thesis, Aarhus University, Denmark, 2016.

Le Quéré, C., Andrew, R. M., Canadell, J. G., Sitch, S., Korsbakken, J. I., Peters, G. P., Manning, A. C., Boden, T. A., Tans, P. P., Houghton, R. A., Keeling, R. F., Alin, S., Andrews, O. D., Anthoni, P., Barbero, L., Bopp, L., Chevallier, F., Chini, L. P., Ciais, P., Currie, K., Delire, C., Doney, S. C., Friedlingstein, P., Gkritzalis, T., Harris, I., Hauck, J., Haverd, V., Hoppema, M., Klein Goldewijk, K., Jain, A. K., Kato, E., Körtzinger, A., Landschützer, P., Lefèvre, N., Lenton, A., Lienert, S., Lombardozzi, D., Melton, J. R., Metzl, N., Millero, F., Monteiro, P. M. S., Munro, D. R., Nabel, J. E. M. S., Nakaoka, S.-I., O'Brien, K., Olsen, A., Omar, A. M., Ono, T., Pierrot, D., Poulter, B., Rödenbeck, C., Salisbury, J., Schuster, U., Schwinger, J., Séférian, R., Skjelvan, I., Stocker, B. D., Sutton, A. J., Takahashi, T., Tian, H., Tilbrook, B., van der Laan-Luijkx, I. T., van der Werf, G. R., Viovy, N., Walker, A. P., Wiltshire, A. J., and Zaehle, S.: Global Carbon Budget 2016, Earth Syst. Sci. Data, 8, 605-649, doi:10.5194/essd-8-605-2016, 2016.

Lee, J.-E., Berry, J. A., van der Tol, C., Yang, X., Guanter, L., Damm, A., Baker, I., and Frankenberg, C.: Simulations of chlorophyll fluorescence incorporated into the Community Land Model version 4, Glob Change Biol, 21, 3469–3477, doi:10.1111/gcb.12948, 2015.

Lohila A., Minkkinen K., Aurela M., Tuovinen J.-P., Penttilä T., Ojanen P., and Laurila, T.: Greenhouse gas flux measurements in a forestry-drained peatland indicate a large carbon sink, Biogeosciences, 8, 3203–3218, 2011.

Luo, Y. Q., Randerson, J. T., Abramowitz, G., Bacour, C., Blyth, E., Carvalhais, N., Ciais, P., Dalmonech, D., Fisher, J. B., Fisher, R., Friedlingstein, P., Hibbard, K., Hoffman, F., Huntzinger, D., Jones, C. D., Koven, C., Lawrence, D., Li, D. J., Mahecha, M., Niu, S. L., Norby, R., Piao, S. L., Qi, X., Peylin, P., Prentice, I. C., Riley, W., Reichstein, M., Schwalm, C., Wang, Y. P., Xia, J. Y., Zaehle, S., and Zhou, X. H.: A framework for benchmarking land models, Biogeosciences, 9, 3857-3874, doi:10.5194/bg-9-3857-2012, 2012.

Meroni, M., Rossini, M., Guanter, L., Alonso, L., Rascher, U., Colombo, R., and Moreno, J.: Remote sensing of solar-induced chlorophyll fluorescence: Review of methods and applications, Remote Sens. Environ., 113, 2037-2051, 2009.

Magnani, F. and Dayyoub, A.: Modelling chlorophyll fluorescence under ambient conditions. In preparation, 2016.

Mammarella I., Launiainen S., Grönholm T., Keronen P., Pumpanen J., Rannik, Ü., and Vesala, T.: Relative humidity effect on the high frequency attenuation of water vapour flux measured by a closed-path eddy covariance system, J. Atmos. Ocean Tech., 26, 1856-1866, 2009.

Markkanen, T., Thum, T., Susiluoto, J., Aurela, M., Gao, Y., Laurila, T., Lehtonen, A., Liski, J., Lohila, A., Mammarella, I., Ťupek, B. and Aalto, T.: Modelling carbon fluxes and pools in Finland and their trends in past decades. In preparation, 2016.

Maxwell, K., and Johnson, G. N.: Chlorophyll fluorescence – a practical guide. Journal of Experimental Botany, 61, 659-668, 2000.

Munro, R., Eisinger, M. Anderson, C., Callies, J., Corpaccioli, E., Lang, R., Lefebvre, A., Livschitz, Y., and Perez Albinana, A.: GOME-2 on MetOp: from in-orbit verification routine to routine operations. In: Proceeding of EUMETSAT Meteorological Satellite Conference, Helsinki, Finland, 12-16 June 2006.

Murchie, E. H. and T. Lawson, 2013. Chlorophyll fluorescence analysis: a guide to good practice and understanding some new applications. Journal of Experimental Botany, doi:10.1093/jxb/ert208.

Norton, A. J., Rayner, P. J., Koffi, E. N., and Scholze, M.: Assimilating solar-induced chlorophyll fluorescence into the terrestrial biosphere model BETHY-SCOPE: Model description and information content, Geosci. Model Dev. Discuss., doi:10.5194/gmd-2017-34, in review, 2017.

Parazoo, N. C., Bowman, K., Fisher, J. B., Frankenberg, C., Jones, D. B. A., Cescatti, A., Pérez-Priego, Ó., Wohlfahrt, G., and Montagnani, L.: Terrestrial gross primary production inferred from satellite fluorescence and vegetation models, Global Change Biol., doi: 10.1111/gcb.12652, 2014.

Parazoo, N. C., Bowman, K., Frankenberg, C., Lee, J.-E., Fisher, J. B., Worden, J., Jones, D. B. A., Berry, J., Collatz, G. J., Baker, I. T., Jung, M., Liu, J., Osterman, G., O'Dell, C., Sparks, A., Butz, A., Guerlet, S., Yoshida, Y., Chen, H., and Gerbig, C.: Interpreting seasonal changes in the carbon balance of southern Amazonia using measurements of XCO_2 and chlorophyll fluorescence from GOSAT, Geophys. Res. Lett., 40, 2829–2833, doi:10.1002/grl.50452, 2013.

Palmroth, S., and Hari, P.: Evaluation of the importance of acclimation of needle structure, photosynthesis, and respiration to available photosynthetically active radiation in a Scots pine canopy, Can. J. For. Res., 31, 1235-1243, 2001.

Pinty, B., Clerici, M., Andredakis, I., Kaminski, T., Taberner, M., Verstraete, M. M., Gobron, N., Plummer, S., and Widlowski, J.-L.: Exploiting the MODIS albedos with the Two-stream Inversion Package (JRC-TIP): 2. Fractions of transmitted and absorbed fluxes in the vegetation and soil layers, J. Geophys. Res., 116, D09106, doi:10.1029/2010JD015373, 2011.

Porcar-Castell, A.: A high resolution portrait of the annual acclimation in photochemical and non-photochemical quenching in needles of Pinus sylvestris, Physiol. Plantarum, 143, 139-153, 2011.

Porcar-Castell, A., Bäck, J., Juurola, E., and Hari, P.: Dynamics of the energy flow through photosystem II under changing light conditions: a model approach, Functional Plant Biology, 33, 229-239, 2006.

Porcar-Castell, A., Pfündel, E., Korhonen, J.F.J., and Juurola, E.: A new monitoring PAM fluorometer (MONI-PAM) to study the short- and long-term acclimation of photosystem II in field conditions, Photosynth. Res., 96, 173-179, 2008.

Porcar-Castell, A., Tyystjärvi, E., Atherton, J., van der Tol, C., Flexas, J., Pfündel, E., Moreno, J., Frankenberg, C., and Berry, J. A.: Linking chlorophyll-a fluorescence to photosynthesis for remote sensing applications: mechanisms and challenges, Journal of Experimental Botany, 65, 4065-4095 doi:10.1093/jxb/eru191, 2014.

Rabinowich, E. and Govindjee: Photosynthesis. John Wiley and Sons, New York, 273 pp, 1969.

Rannik, Ü., Keronen, P., Hari, P., and Vesala, T.: Estimation of forest-atmosphere CO_2 exchange by eddy covariance and profile techniques, Agr. Forest Meteorol., 126, 141-155, 2004.

Rannik, Ü., Peltola, O., and Mammarella, I.: Random uncertainties of flux measurements by the eddy covariance technique, Atmos. Meas. Tech., 9, 5163-5181, doi:10.5194/amt-9-5163-2016, 2016.

Reick C.H., Raddatz T., Brovkin V., and Gayler, V.: Representation of natural and anthropogenic land cover change in MPI-ESM, J. Adv. Model. Earth Syst., 5, 459-482, 2013.

Ruosteenoja, K., Raisanen, J. and Pirinen, P.: Projected changes in thermal seasons and the growing season in Finland, Int. J. Climatol., 31, 1473–1487, 2011.

Schaefer, K., et al.: A model-data comparison of gross primary productivity: Results from the North American Carbon Program site synthesis, J. Geophys. Res., 117, G03010, doi:10.1029/2012JG001960, 2012.

Sellers, P.J.: Canopy reflectance, photosynthesis and transpiration, Int. J. Remote Sens., 6, 1335-1372, 1985.

Sitch, S., Friedlingstein, P., Gruber, N., Jones, S. D., Murray-Tortarolo, G., Ahlström, A., Doney, S. C., Graven, H., Heinze, C., Huntingford, C., Levis, S., Levy, P. E., Lomas, M., Poulter, B., Viovy, N., Zaehle, S., Zeng, N., Arneth, A., Bonan, G., Bopp, L., Canadell, J. G., Chevallier, F., Ciais, P., Ellis, R., Gloor, M., Peylin, P., Piao, S. L., Le Quéré, C., Smith, B., Zhu, Z., and Myneni, R.: Recent trends and drivers of regional sources and sinks of carbon dioxide, Biogeosciences, 12, 653-679, doi:10.5194/bg-12-653-2015, 2015.

Thum, T., Aalto, T., Laurila, T., Aurela, M., Hatakka, J., Lindroth, A., and Vesala, T.: Spring initiation and autumn cessation of boreal coniferous forest CO2 exchange assessed by meteorological and biological variables, Tellus 61B, 701-717, 2009.

Thum, T., Aalto, T., Laurila, T., Aurela, M., Kolari, P., and Hari, P.: Parametrization of two photosynthesis models at the canopy scale in a northern boreal Scots pine forest, Tellus B, 59, 874-890, 2007.

Thum, T., Aalto, T., Laurila, T., Aurela, M., Lindroth, A., and Vesala, T.: Assessing seasonality of biochemical CO_2 exchange model parameters from micrometeorological flux observations at boreal coniferous forest, Biogeosciences, 5, 1625-1639, doi:10.5194/bg-5-1625-2008, 2008.

Thum, T., Aalto, T., Aurela, M., Laurila, T., and Zaehle, S.: Improving the modeling of the seasonal carbon cycle of the boreal forest with chlorophyll fluorescence measurements, in preparation, 2017.

Törmä, M., Hatunen, S., Härmä, P., Markkanen, T., and Mattila O.-P.: Land cover data for carbon balance modeling, Boreal Environ. Res., 20, 243–260, 2015.

Ueyama, M., Tahara, N., Iwata, H., Euskirchen, E.S., Ikawa, H., Koyayashi, , Nagano, H., Nakai, T., and Harazono, Y.: Optimization of a biochemical model with eddy covariance measurements in black spruce forests of Alaska for estimating CO_2 fertilization effects, Agr. Forest Meteorol., 222, 98-111, 2016.

Van Der Tol, C., Berry, J. A., Campbell, P. K. E., and Rascher, U.: Models of fluorescence and photosynthesis for interpreting measurements of solar-induced chlorophyll fluorescence, J. Geophys. Res. Biogeosci., 119, doi:10.1002/2014JG002713, 2014.

Van Der Tol, C., Verhoef, W., and Rosema, A.: A model for chlorophyll fluorescence and photosynthesis at leaf scale, Agr. Forest Meteorol., 149, 96-105, 2009a.

Van Der Tol, C., Verhoef, W., Timmermans, J., Verhoef, A., and Su, Z.: An integrated model of soil-canopy spectral radiances, photosynthesis, fluorescence, temperature and energy balance, Biogeosciences, 6, 3109-3129, doi:10.5194/bg-6-3109-2009, 2009.

Walters, R.G., and Horton, P.: Theoretical assessment of alternative mechanisms for non-photochemical quenching of PS II fluorescence in barley leaves, Photosynth. Res., 36, 119-139, 1993.

Walther, S., Voigt, M., Thum, T., Gonsamo, A., Zhang, Y., Köhler, P., Jung, M., Varlagin, A. and Guanter, L.: Satellite chlorophyll fluorescence measurements reveal large-scale decoupling of photosynthesis and greenness dynamics in boreal evergreen forests, Global Change Biol., 22, 2979–2996, doi:10.1111/gcb.13200, 2016.

Wang, K. Y., Kellomäki, S., and Laitinen, K.: Acclimation of photosynthetic parameters in Scots pine after three-year exposure to elevated CO_2 and temperature, Agr. Forest Meteorol., 82, 195–217, 1996.

Wohlfahrt, G. and Galvano, M.: Revisiting the choice of the driving temperature for eddy covariance CO_2 flux partitioning, Agric. Forest. Met., 237-238, 135-142, 2017.

Yang, X., Tang, J., Mustard, J. F., Lee, J.-E., Rossini, M., Joiner, J., Munger, J. W., Kornfeld, A., and Richardson, A. D.: Solar-induced chlorophyll fluorescence that correlates with canopy photosynthesis on diurnal and seasonal scales in a temperate deciduous forest. Geophys. Res. Lett., 42, 2977–2987. doi: 10.1002/2015GL063201, 2015.

Tables

Table 1. Measurement sites

Abbreviation	Name	Location	Vegetation	total LAI [m^2 m^{-2}]	Year	Reference
FI-Kns	Kalevansuo	60°39'N 24°21'E	Scots pine forest	5	2007-2008	Lohila *et al.* (2011)
FI-Hyy	Hyytiälä	61°51'N 24°18'E	Scots pine forest	6	2007-2011	Rannik *et al.* (2004) Mammarella *et al.* (2009)
FI-Ken	Kenttärova	67°59'N 24°15'E	Norway spruce forest	6.6	2007-2011	Thum *et al.* (2008) Aurela *et al.* (2016)

FI-Sod	Sodankylä	67°21ˈN 26°38ˈE	Scots pine forest	3.6	2007-2008	Thum *et al.* (2007)

Table 2. The correlation coefficient (r^2) and its significance (in parenthesis) between modelled and observed sun-induced fluorescence (SIF) (observed SIF in units mW m^{-2} sr^{-1} nm^{-1}) and gross primary production (GPP) (unit: g C m^{-2} day^{-1}) values at different sites. In the calculation of linear regressions between simulated and observed GPP and SIF, 20-day time periods and the morning values were used. In the calculation of GPP vs. fraction of absorbed photosynthetic active radiation by the vegetation (fAPAR) fits, monthly values including the whole day were used.

	FI-Kns	FI-Hyy	FI-Sod	FI-Ken
Obs. GPP vs. obs. SIF	0.91 ~~0.89~~	0.93 ~~0.92~~	0.89 ~~0.83~~	0.82 ~~0.83~~
	$(8.82\cdot10^{-18})$	$(1.07\cdot10^{-48})$	$(5.70\cdot10^{-12})$	$(3.14\cdot10^{-30})$
	$(3.66\cdot10^{-19})$	$(4.24\cdot10^{-51})$	$(3.44\cdot10^{-11})$	$(7.33\cdot10^{-22})$
Mod. GPP vs. mod. SIF	0.99	0.92	0.99	0.83
	$(1.20\cdot10^{-34})$	$(5.80\cdot10^{-85})$	$(1.04\cdot10^{-29})$	$(1.38\cdot10^{-29})$
Obs. GPP vs. mod. GPP	0.97	0.98	0.84	0.82
	$(1.25\cdot10^{-27})$	$(8.02\cdot10^{-73})$	$(2.06\cdot10^{-12})$	$(2.40\cdot10^{-29})$
Obs. SIF vs. mod. SIF	~~0.88~~	~~0.89~~	~~0.63~~	~~0.79~~
	0.90	0.90	0.66	0.81
	~~$(3.70\cdot10^{-17})$~~	~~$(6.85\cdot10^{-43})$~~	~~$(2.21\cdot10^{-7})$~~	~~$(3.63\cdot10^{-26})$~~
	$(4.00\cdot10^{-18})$	$(3.03\cdot10^{-44})$	$(3.41\cdot10^{-18})$	$(9.17\cdot10^{-28})$
Obs. GPP vs. obs. fAPAR	0.90	0.66	0.82	0.72
	$(5.64\cdot10^{-10})$	$(1.68\cdot10^{-12})$	$(6.16\cdot10^{-8})$	$(1.01\cdot10^{-13})$
Mod. GPP vs. mod. fAPAR	0.89	0.86	0.80	0.67
	$(3.01\cdot10^{-12})$	$(4.98\cdot10^{-27})$	$(2.33\cdot10^{-9})$	$(5.82\cdot10^{-16})$
Obs. fAPAR vs. mod. fAPAR	0.77	0.70	0.72	0.67
	$(1.58\cdot10^{-8})$	$(8.26\cdot10^{-17})$	$(1.53\cdot10^{-7})$	$(1.31\cdot10^{-15})$

Table 3. The slopes of the fits between gross primary production (GPP) and sun-induced chlorophyll fluorescence (SIF)/ fraction of absorbed photosynthetic active radiation by vegetation (fAPAR). Note that a constant scalar was used in multiplying the modelled SIF values.

	FI-Kns	FI-Hyy	FI-Sod	FI-Ken	Average	Standard deviation
Obs. GPP vs. obs. SIF	~~8.3~~	~~10~~	~~11~~	~~9.8~~		
	7.6 (±0.4)	9.8 (±0.3)	9.5 (±0.7)	7.8 (±0.5)	8.7	1.0
Mod. GPP vs. mod. SIF	8.3 (±0.1)	9.7~~6~~ (±0.1)	8.5 (±0.1)	9.2~~1~~ (±0.5)	8.9	0.5
Obs. GPP vs. obs. fAPAR	22.9 (±2.5)	24.1 (±2.5)	13.2 (±1.5)	12.5 (±1.2)	18.2	5.3
Mod. GPP vs. mod. fAPAR	15.8 (±1.2)	18.1~~6~~ (±0.9)	5.8 (±0.6)	4.3~~2~~ (±0.4)	11.0	6.0

Table A1. Descriptions of the variables and parameters.

Variable/Parameter (unit)	Description	Value	Reference
Φ_p	Yield for photochemistry		
Φ_f	Yield for fluorescence		
Φ_D	Yield for energy-independent heat dissipation		
Φ_{NPQ}	Yield for energy-dependent heat dissipation		
k_p (s^{-1})	Rate constant of photochemistry		
k_f (s^{-1})	Rate constant of fluorescence	$6.7 \cdot 10^7$	Rabinowich and Govindjee (1969)
k_D (s^{-1})	Rate constant of energy-independent heat dissipation	$6.03 \cdot 10^8$	Porcar-Castell et al. (2006)
k_{NPQ} (s^{-1})	Rate constant of energy-dependent heat dissipation		
k_{PSII} (s^{-1})	Intrinsic rate of photochemistry		

qL_T	Photochemical quenching parameter (representing the fraction of functional and open reaction centers)		
qL_r	The fraction of open reaction centers		
qL_s	The fraction of functional reaction centers		
k_{NPQr} (s^{-1})	Rate constant of reversible component of k_{NPQ}		
k_{NPQs} (s^{-1})	Rate constant of sustained component of k_{NPQ}		
J_a (μmol m^{-2} s^{-1})	Actual electron transport rate		
A (μmol m^{-2} s^{-1})	Photosynthesis		
A_j (μmol m^{-2} s^{-1})	Electron transport rate limited photosynthesis		
A_c (μmol m^{-2} s^{-1})	Maximum carboxylation rate limited photosynthesis		
J_{max} (μmol m^{-2} s^{-1})	Maximum potential electron transport rate		
$\Phi_{f,0}$	Dark-adapted fluorescence yield of PSII		
$\Phi_{p,max}$ (mol / E)	Maximum quantum yield of PSII in dark-acclimated conditions in the absence of stress	0.88	Pfundel (1998)

Figure captions

Fig. 1. a) The annual cycles (15.8.2008-14.8.2009) of measured chlorophyll fluorescence (F' and photochemical yield Φ_p) (ChlF, MONI-PAM) and gross primary production (GPP) together with the simulated ChlF variables (SIF and fluorescence yield $\Phi_{f,s}$) and GPP from the JSBACH model at a daily scale at site FI-Hyy. All the ChlF variables are scaled from zero to one. The thick line for the modelled ChlF values is a 15-day running average of the value. b) The modelled and observed gross primary production (GPP) at half-hourly means (dots) and corresponding 30-day running mean (thick lines).

Fig. 2. The daily cycle of simulated SIF and $\Phi_{f,s}$ in three different canopy layers of JSBACH on day 160 in 2008. Layer 1 was the upmost layer without attenuation taken into account in a) and b) and with attenuation estimated from the SCOPE model included in e) and f). The sums of different layers are shown in c) (SIF) and d) ($\Phi_{f,s}$) with and without attenuation.

Fig. 3. Observed and simulated SIF and GPP scaled to unity (unitless) with corresponding standard deviations at a) FI-Kns, c) FI-Hyd, e) FI-Sod, g) FI-Ken.

Fig. 4. Maps for our study region with GOME-SIF, JSBACH-SIF, JSBACH-GPP and MPI BGC-GPP averaged for time period 2007–2011 and separated between seasons.

Fig. 5. Latitudinal transect at 28°E showing JSBACH-GPP, MPI-BGC-GPP and observed and simulated SIF averaged for the time period 2007–2008. All quantities have been scaled to unity.

Fig. 6. Correlation plots for different seasons, GOME-SIF vs. JSBACH-SIF. Note that JSBACH-SIF has been multiplied by 100.

Fig. 7. Averaged seasonal cycles of observed and simulated SIF (a) and MPI-BGC and simulated GPP (b) separated by latitudinal regions. Note that the simulated SIF value was multiplied by 100. The observed SIF is in units mW m^{-2} sr^{-1} nm^{-1}.

Figures

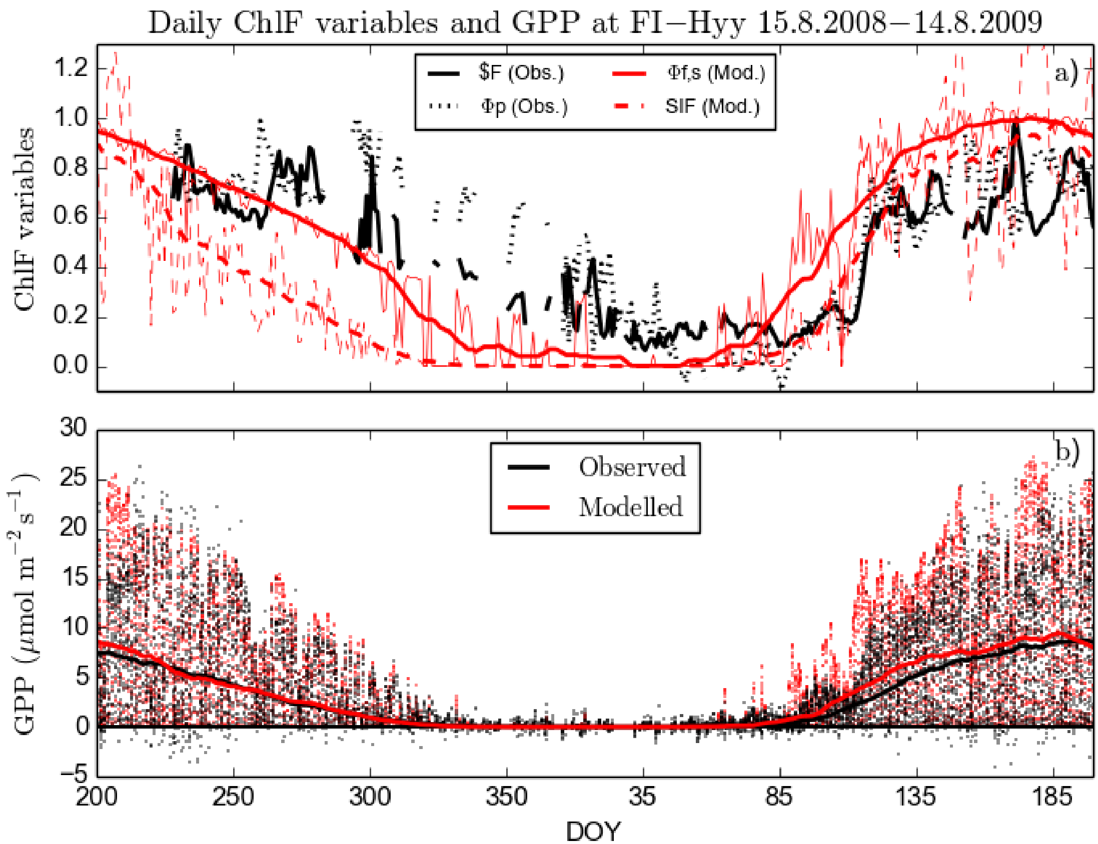
Daily ChlF variables and GPP at FI−Hyy 15.8.2008−14.8.2009
ChlF variables
$F (Obs.)
Φp (Obs.)
Φf,s (Mod.)
SIF (Mod.)
a)
GPP (μmol m−2 s−1)
Observed
Modelled
b)
DOY
200
250
300
350
35
85
135
185

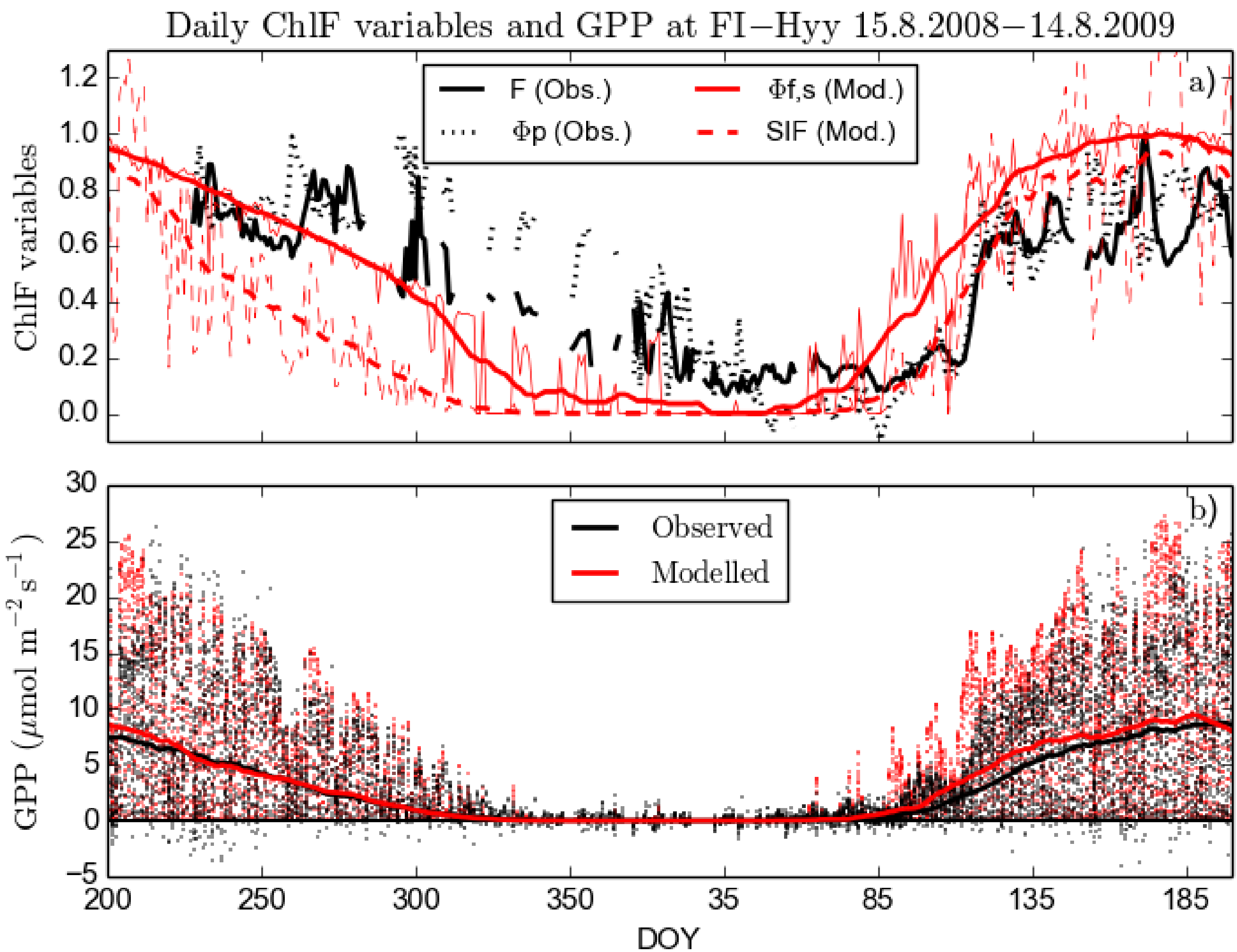

Daily ChlF variables and GPP at FI−Hyy 15.8.2008−14.8.2009
F (Obs.)
Φp (Obs.)
Φf,s (Mod.)
SIF (Mod.)
a)
ChlF variables
1.2
1.0
0.8
0.6
0.4
0.2
0.0
Observed
Modelled
b)
GPP (μmol m−2 s−1)
30
25
20
15
10
5
0
−5
200
250
300
350
35
85
135
185
DOY

Fig. 1

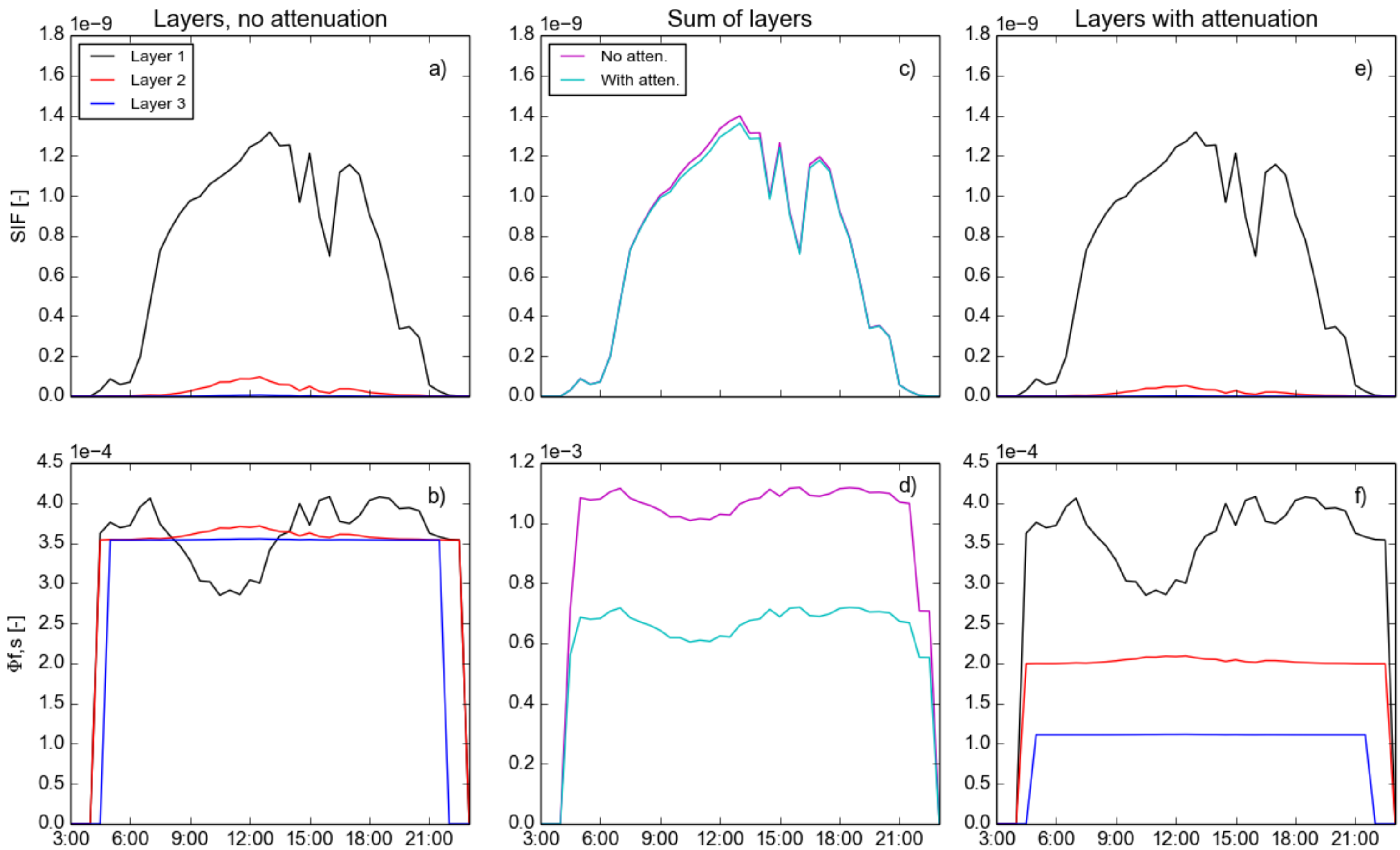

Layers, no attenuation
Sum of layers
Layers with attenuation
1e−9
1e−4
1e−3
Layer 1
Layer 2
Layer 3
No atten.
With atten.
a)
b)
c)
d)
e)
f)
SIF [-]
Φf,s [-]
3:00
6:00
9:00
12:00
15:00
18:00
21:00

Fig. 2

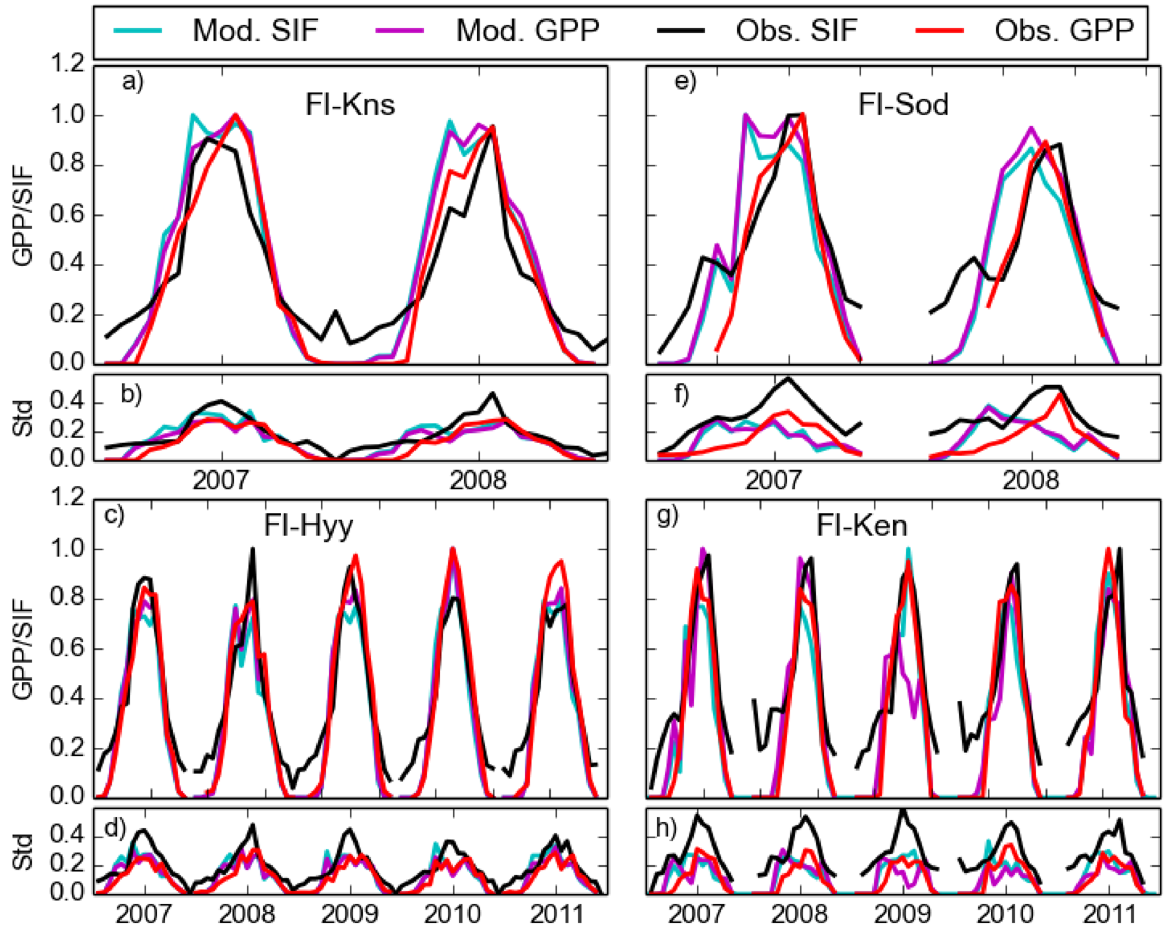

Mod. SIF
Mod. GPP
Obs. SIF
Obs. GPP
a)
FI-Kns
b)
c)
FI-Hyy
d)
e)
FI-Sod
f)
g)
FI-Ken
h)
GPP/SIF
Std
1.2
1.0
0.8
0.6
0.4
0.2
0.0
2007
2008
2009
2010
2011

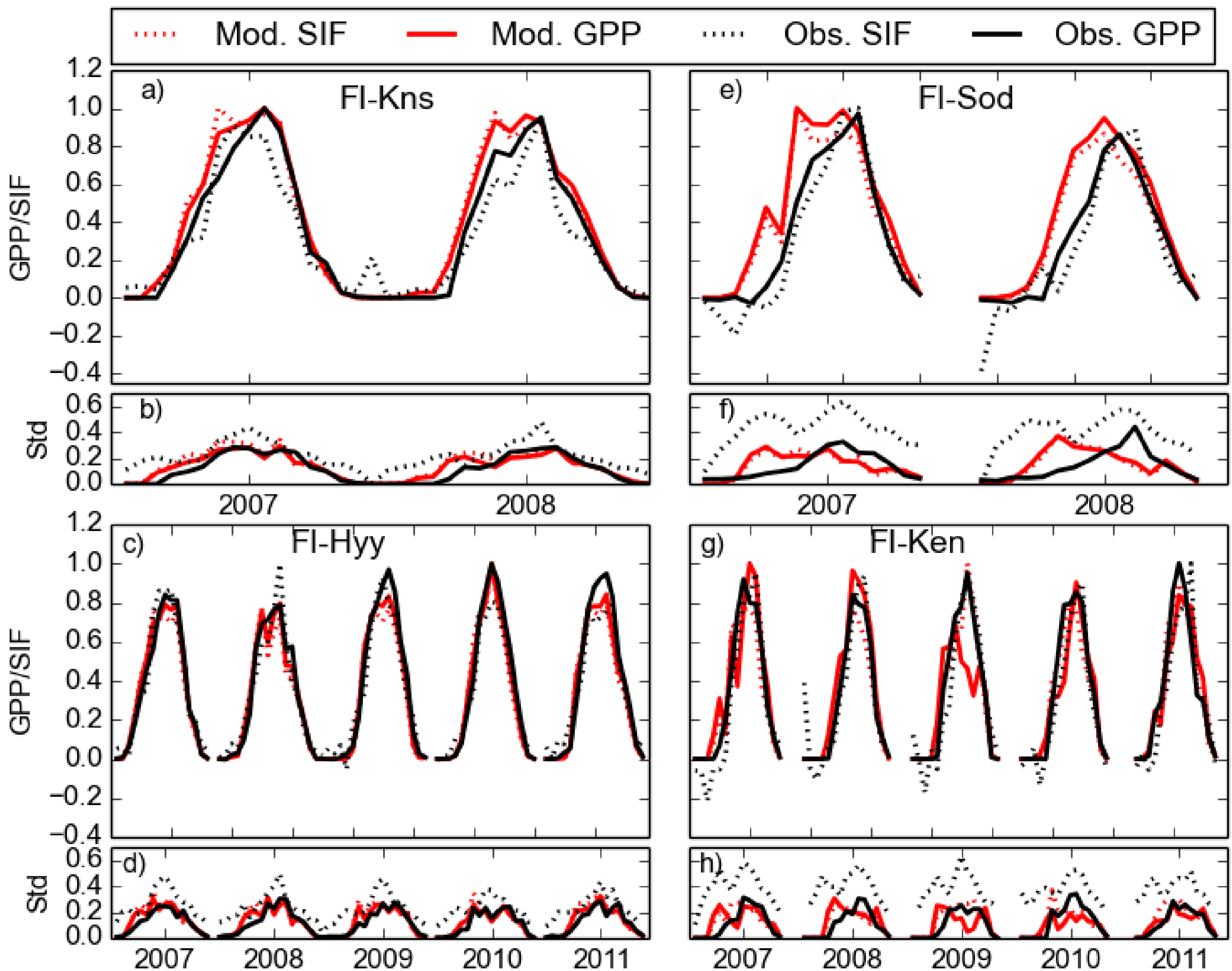

Mod. SIF
Mod. GPP
Obs. SIF
Obs. GPP
a)
FI-Kns
e)
FI-Sod
b)
f)
c)
FI-Hyy
g)
FI-Ken
d)
h)
GPP/SIF
Std
2007
2008
2009
2010
2011
1.2
1.0
0.8
0.6
0.4
0.2
0.0
−0.2
−0.4

Fig. 3

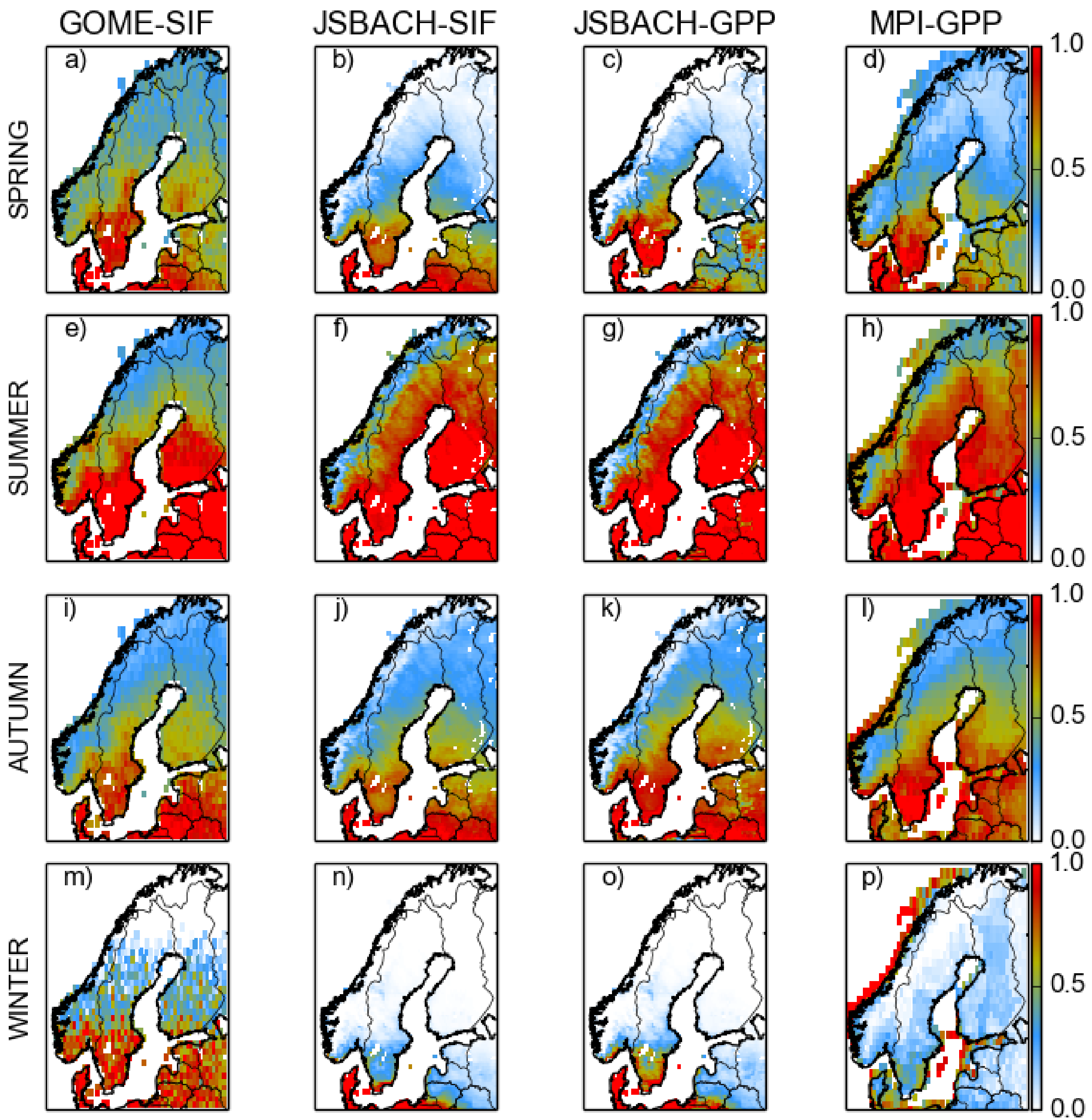
GOME-SIF
JSBACH-SIF
JSBACH-GPP
MPI-GPP
SPRING
SUMMER
AUTUMN
WINTER
a)
b)
c)
d)
e)
f)
g)
h)
i)
j)
k)
l)
m)
n)
o)
p)
1.0
0.5
0.0

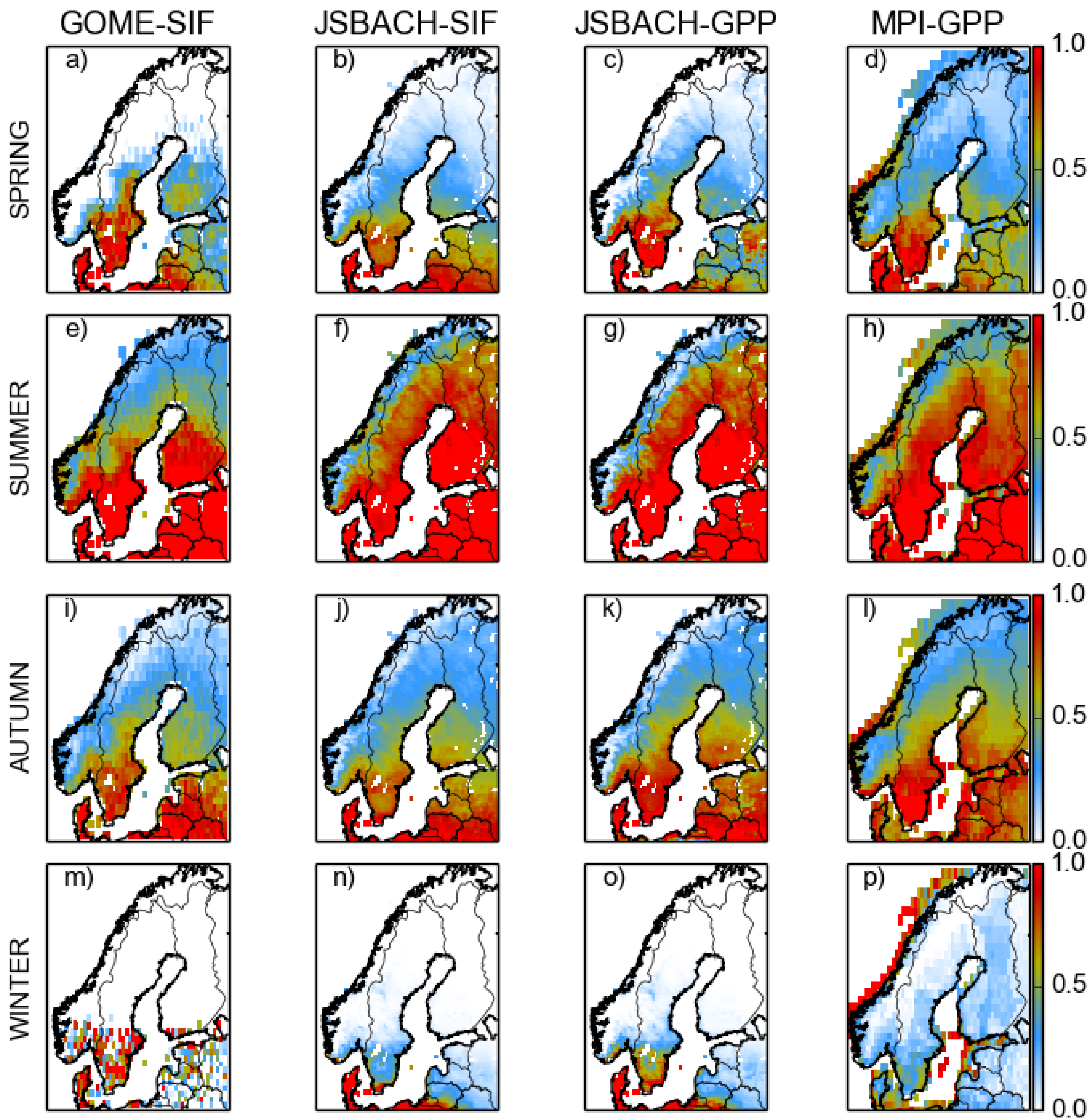
GOME-SIF
JSBACH-SIF
JSBACH-GPP
MPI-GPP
SPRING
SUMMER
AUTUMN
WINTER
a)
b)
c)
d)
e)
f)
g)
h)
i)
j)
k)
l)
m)
n)
o)
p)
1.0
0.5
0.0

Fig. 4

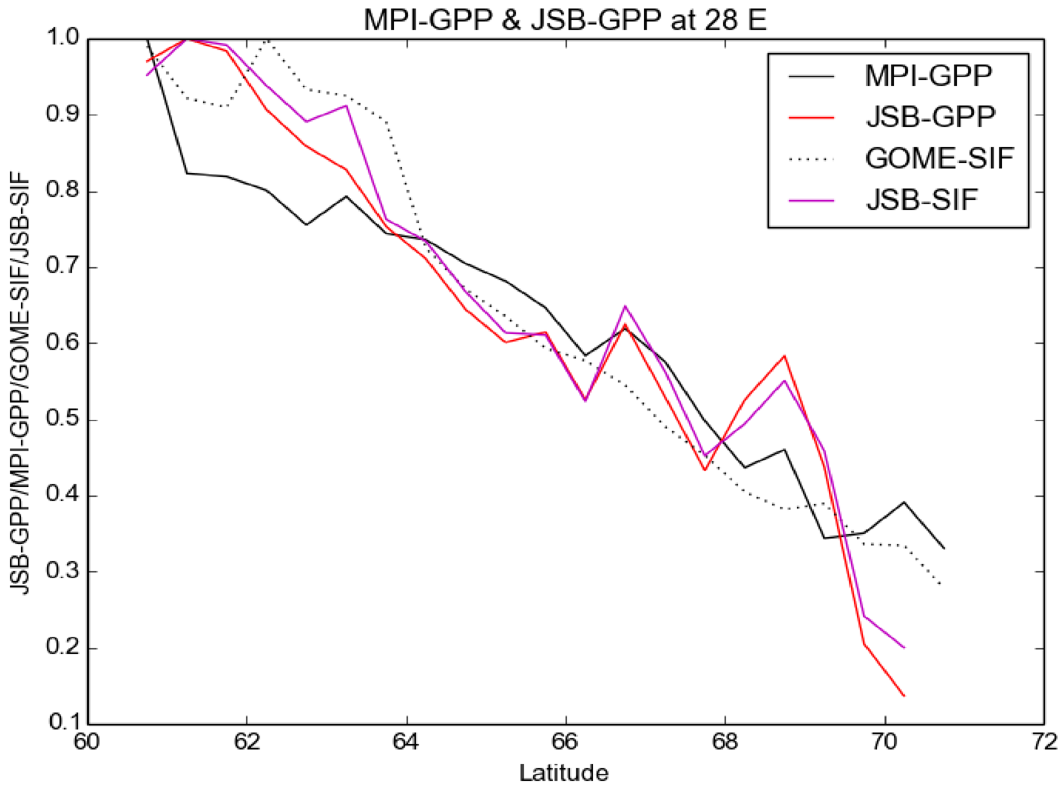

MPI-GPP & JSB-GPP at 28 E
JSB-GPP/MPI-GPP/GOME-SIF/JSB-SIF
Latitude
MPI-GPP
JSB-GPP
GOME-SIF
JSB-SIF
1.0
0.9
0.8
0.7
0.6
0.5
0.4
0.3
0.2
0.1
60
62
64
66
68
70
72

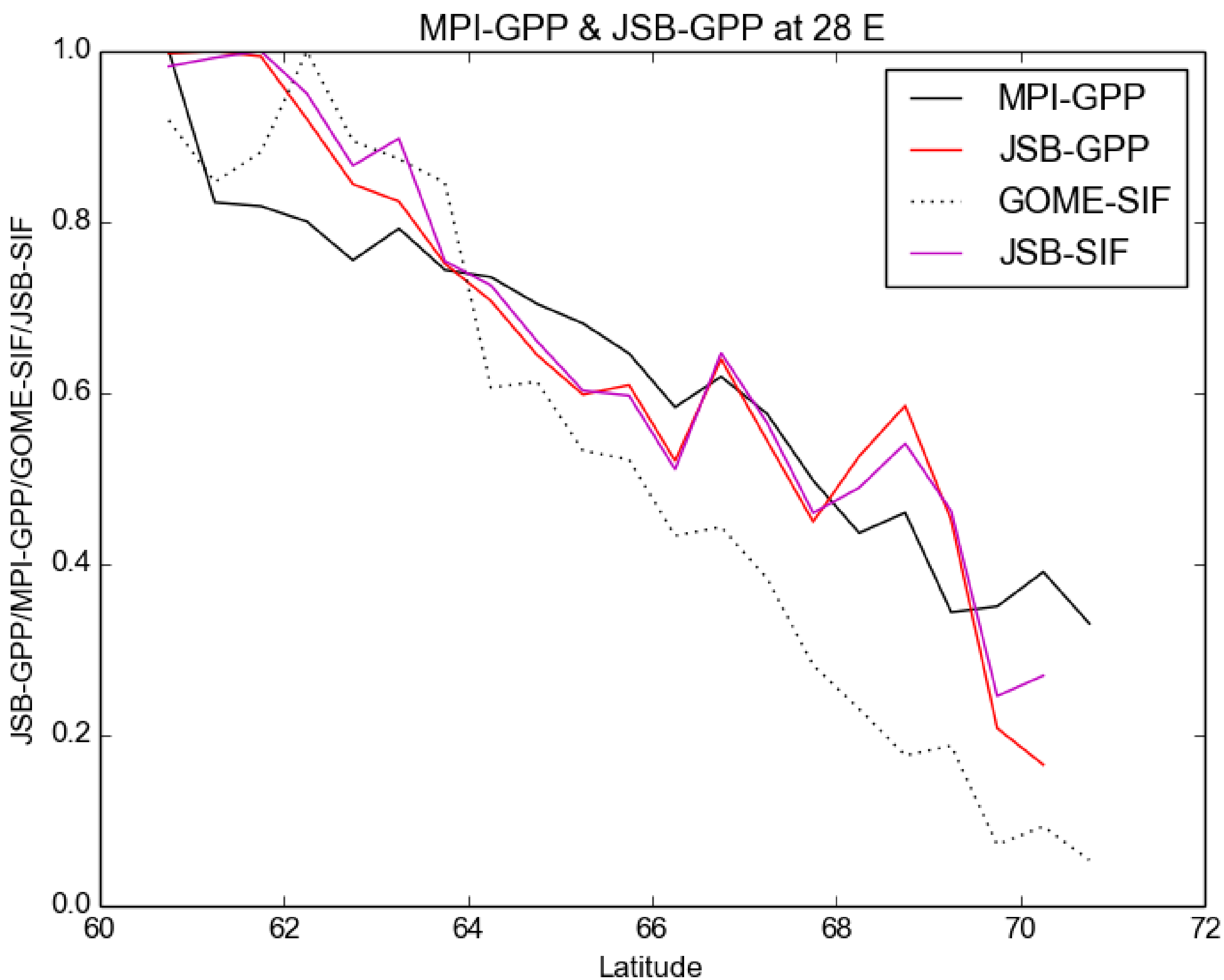
MPI-GPP & JSB-GPP at 28 E
MPI-GPP
JSB-GPP
GOME-SIF
JSB-SIF
JSB-GPP/MPI-GPP/GOME-SIF/JSB-SIF
Latitude
1.0
0.8
0.6
0.4
0.2
0.0
60
62
64
66
68
70
72

Fig. 5

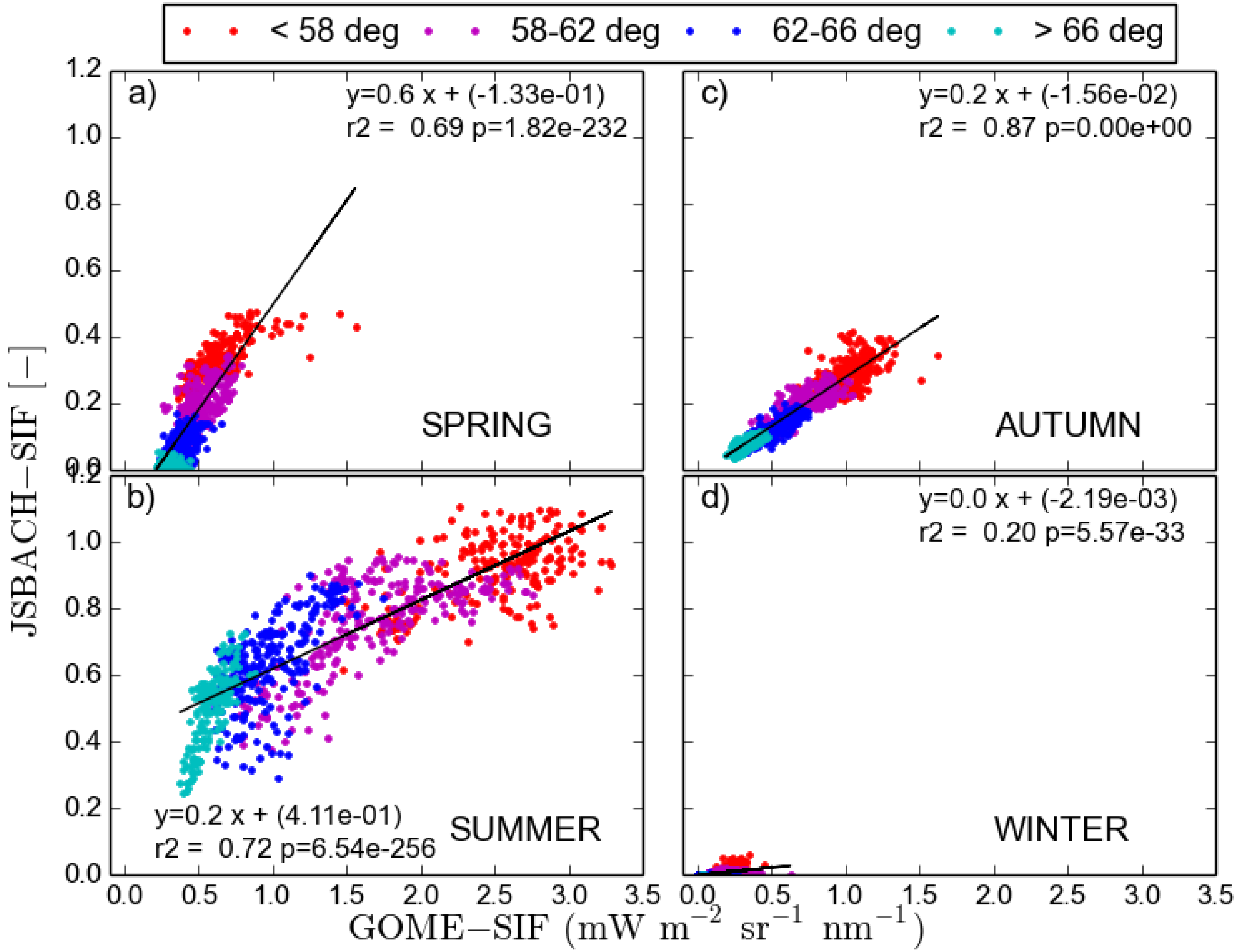

< 58 deg
58-62 deg
62-66 deg
> 66 deg
a)
y=0.6 x + (-1.33e-01)
r2 = 0.69 p=1.82e-232
SPRING
b)
y=0.2 x + (4.11e-01)
r2 = 0.72 p=6.54e-256
SUMMER
c)
y=0.2 x + (-1.56e-02)
r2 = 0.87 p=0.00e+00
AUTUMN
d)
y=0.0 x + (-2.19e-03)
r2 = 0.20 p=5.57e-33
WINTER
JSBACH−SIF [−]
GOME−SIF (mW m−2 sr−1 nm−1)

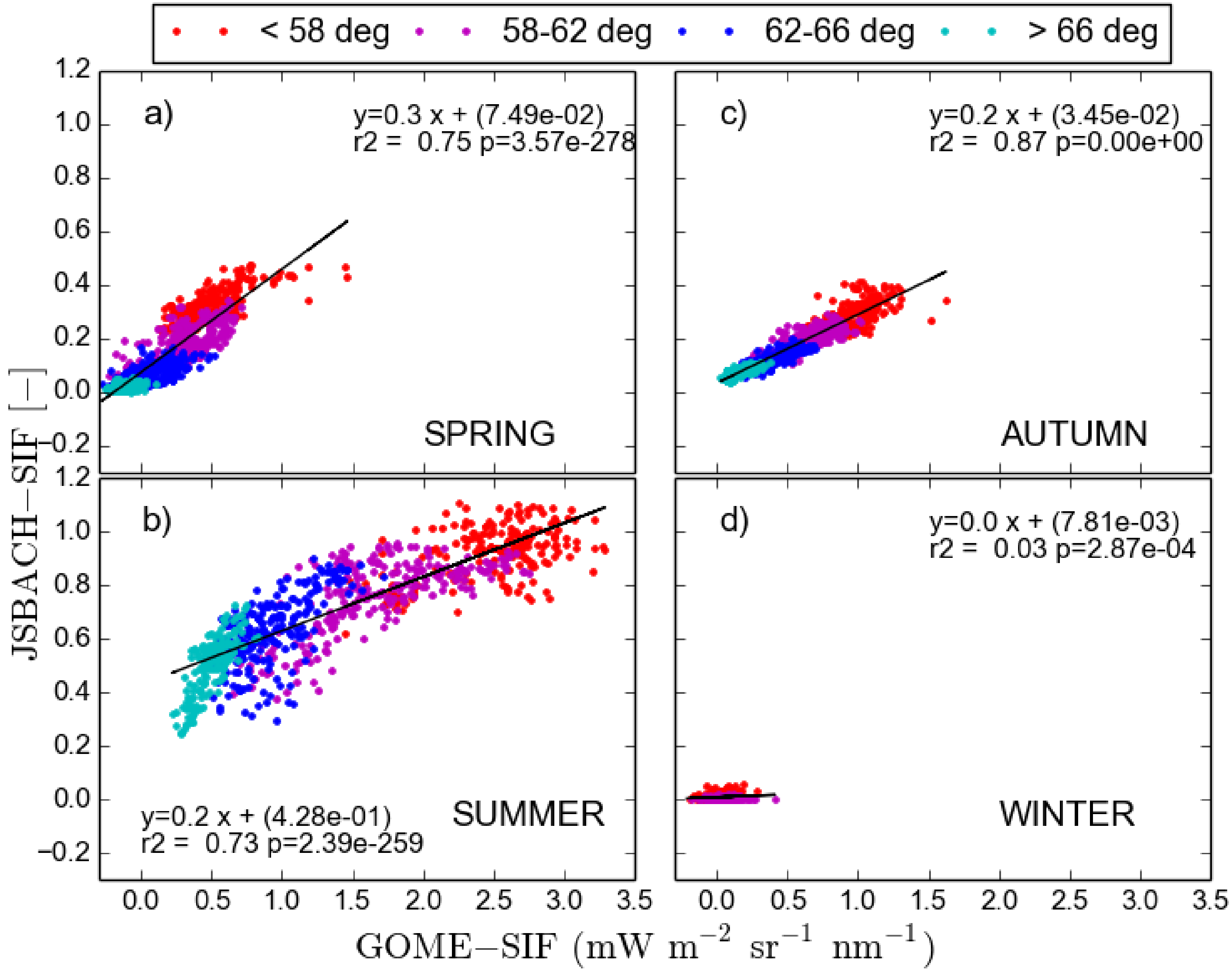
< 58 deg
58-62 deg
62-66 deg
> 66 deg
a)
y=0.3 x + (7.49e-02)
r2 = 0.75 p=3.57e-278
SPRING
c)
y=0.2 x + (3.45e-02)
r2 = 0.87 p=0.00e+00
AUTUMN
b)
y=0.2 x + (4.28e-01)
r2 = 0.73 p=2.39e-259
SUMMER
d)
y=0.0 x + (7.81e-03)
r2 = 0.03 p=2.87e-04
WINTER
JSBACH−SIF [−]
GOME−SIF (mW m⁻² sr⁻¹ nm⁻¹)

Fig. 6

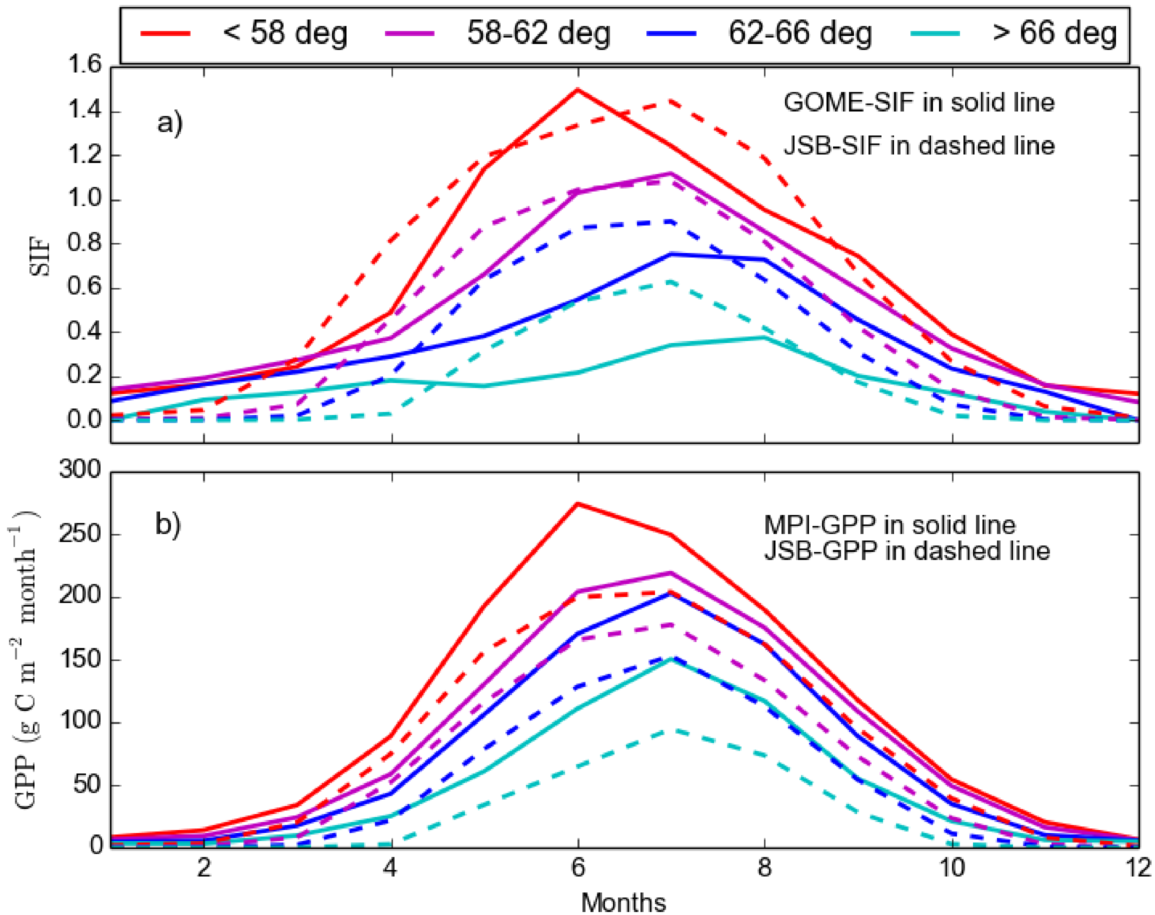
< 58 deg
58-62 deg
62-66 deg
> 66 deg
a)
GOME-SIF in solid line
JSB-SIF in dashed line
SIF
b)
MPI-GPP in solid line
JSB-GPP in dashed line
GPP (g C m⁻² month⁻¹)
Months

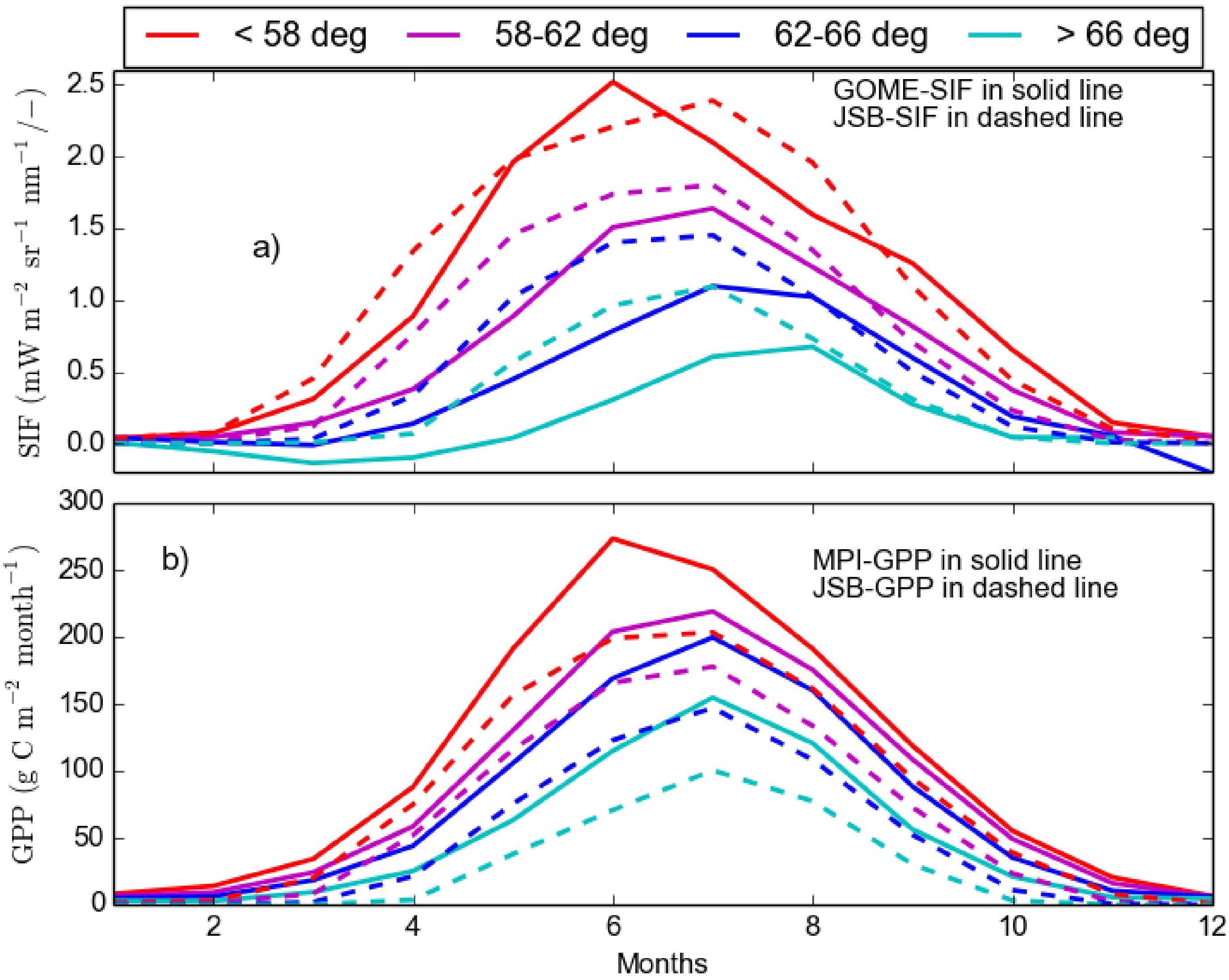
< 58 deg
58-62 deg
62-66 deg
> 66 deg
GOME-SIF in solid line
JSB-SIF in dashed line
a)
SIF (mW m^-2 sr^-1 nm^-1 /—)
2.5
2.0
1.5
1.0
0.5
0.0
b)
MPI-GPP in solid line
JSB-GPP in dashed line
GPP (g C m^-2 month^-1)
300
250
200
150
100
50
0
2
4
6
8
10
12
Months

Fig. 7